NAVAL POSTGRADUATE SCHOOL

MONTEREY, CALIFORNIA

THESIS

MEMS-BASED WASTE VIBRATIONAL ENERGY HARVESTERS

by

Daniel B. Hogue
Sarah M. Gregory

June 2013

Thesis Advisor: Dragoslav Grbovic
Second Reader: Gamani Karunasiri

Approved for public release; distribution is unlimited

THIS PAGE INTENTIONALLY LEFT BLANK

REPORT DOCUMENTATION PAGE		*Form Approved OMB No. 0704-0188*

1. AGENCY USE ONLY *(Leave blank)*	**2. REPORT DATE** June 2013	**3. REPORT TYPE AND DATES COVERED** Master's Thesis

4. TITLE AND SUBTITLE MEMS-BASED WASTE VIBRATIONAL ENERGY HARVESTERS	**5. FUNDING NUMBERS**
6. AUTHOR(S) Daniel B. Hogue, Sarah M. Gregory	

7. PERFORMING ORGANIZATION NAME(S) AND ADDRESS(ES) Naval Postgraduate School Monterey, CA 93943-5000	**8. PERFORMING ORGANIZATION REPORT NUMBER**

9. SPONSORING /MONITORING AGENCY NAME(S) AND ADDRESS(ES) Marine Corps Expeditionary Energy Office Headquarters Marine Corps Washington, DC 20380-1775	**10. SPONSORING/MONITORING AGENCY REPORT NUMBER** RPGY3

11. SUPPLEMENTARY NOTES The views expressed in this thesis are those of the author and do not reflect the official policy or position of the Department of Defense or the U.S. government. IRB Protocol number ____NA____.

12a. DISTRIBUTION / AVAILABILITY STATEMENT Approved for public release; distribution is unlimited	**12b. DISTRIBUTION CODE** A

13. ABSTRACT (maximum 200 words)
The piezoelectric effect is a phenomenon where strain on a piezoelectric crystal structure causes potential difference at its ends. By merging piezoelectric materials and microelectromechanical systems (MEMS), mechanical vibration could cause the necessary displacement in MEMS to create a potential difference that could be used to power electronic devices. Developing new sustainable energy sources and using energy more efficiently is at the forefront of several research initiatives and is a clear priority for the Department of the Navy's strategic planning. This thesis aims to design a vibrational energy harvesting MEMS device to harness vibrational waste energy with the goal of producing power for naval applications. The development and widespread use of vibrational harvesting MEMS would aid the effort to meet each of these goals in the Department of the Navy. Any shore based, seagoing, or expeditionary mechanical platform could serve as a kinetic energy source for vibration energy harvesting MEMS. This thesis investigates the physics, materials, design, optimization, and microfabrication process in the creation of such a device. Time-dependent finite element models for two designs have been developed, simulating electrical power output. Microfabrication processes for the designs have also been developed.

14. SUBJECT TERMS Energy harvesting, MEMS, piezoelectric	**15. NUMBER OF PAGES** 75
	16. PRICE CODE

17. SECURITY CLASSIFICATION OF REPORT Unclassified	**18. SECURITY CLASSIFICATION OF THIS PAGE** Unclassified	**19. SECURITY CLASSIFICATION OF ABSTRACT** Unclassified	**20. LIMITATION OF ABSTRACT** UU

i

THIS PAGE INTENTIONALLY LEFT BLANK

MEMS-BASED WASTE VIBRATIONAL ENERGY HARVESTERS

Daniel B. Hogue
Lieutenant, United States Navy
B.S., Austin Peay State University, 2007
M.S., Auburn University, 2010

Sarah M. Gregory
Lieutenant Junior Grade, United States Navy
B.S., United States Naval Academy, 2009

Submitted in partial fulfillment of the
requirements for the degree of

MASTER OF SCIENCE IN PHYSICS

from the

**NAVAL POSTGRADUATE SCHOOL
June 2013**

Author: Daniel B. Hogue
                Sarah M. Gregory

Approved by: Dragoslav Grbovic
                Thesis Advisor

                Gamani Karunasiri
                Second Reader

                Andres Larraza
                Chair, Department of Physics

THIS PAGE INTENTIONALLY LEFT BLANK

ABSTRACT

The piezoelectric effect is a phenomenon where strain on a piezoelectric crystal structure causes potential difference at its ends. By merging piezoelectric materials and microelectromechanical systems (MEMS), mechanical vibration could cause the necessary displacement in MEMS to create a potential difference that could be used to power electronic devices. Developing new sustainable energy sources and using energy more efficiently is at the forefront of several research initiatives and is a clear priority for the Department of the Navy's strategic planning. This thesis aims to design a vibrational energy harvesting MEMS device to harness vibrational waste energy with the goal of producing power for naval applications. The development and widespread use of vibrational harvesting MEMS would aid the effort to meet each of these goals in the Department of the Navy. Any shore based, seagoing, or expeditionary mechanical platform could serve as a kinetic energy source for vibration energy harvesting MEMS. This thesis investigates the physics, materials, design, optimization, and microfabrication process in the creation of such a device. Time-dependent finite element models for two designs have been developed, simulating electrical power output. Microfabrication processes for the designs have also been developed.

THIS PAGE INTENTIONALLY LEFT BLANK

TABLE OF CONTENTS

LIST OF FIGURES

LIST OF TABLES

THIS PAGE INTENTIONALLY LEFT BLANK

LIST OF ACRONYMS AND ABBREVIATIONS

AlN   Aluminum Nitride

MEMS   Microelectromechanical Systems

NPS   Naval Postgraduate School

ORNL   Oak Ridge National Laboratory

PiezoMUMPS   Piezoelectric Multi-User MEMS Processes

PZT   Lead Zirconate Titanate

SEM   Scanning Electron Microscopy

SiO_2 Silicon Dioxide

SOI   Silicon on Insulator

XRD   X-ray Diffraction

THIS PAGE INTENTIONALLY LEFT BLANK

ACKNOWLEDGMENTS

THIS PAGE INTENTIONALLY LEFT BLANK

I.   INTRODUCTION

This objective of this thesis is to develop, test, and evaluate a MEMS device comprised of aluminum nitride (AlN) and silicon (Si) in order to make an energy-harvesting piezoelectric generator. Arrays of multitudes of such devices, multiplying the power output of individual devices, could be used to recapture some of the waste vibrational energy from vibrating objects such as engines or machinery.

A.   BACKGROUND

Developing new sustainable energy sources and increasing current energy efficiencies is at the forefront of several research initiatives and is a clear priority for the Department of the Navy's strategic planning. By Executive Order 13514 in October 2009, the Department of the Navy is required to reduce the fleet's total consumption of petroleum products by a minimum of 2 percent annually through the end of FY2020 [1]. The USMC Expeditionary Energy Strategy, issued in March 2011, states:

> By 2025 we will deploy Marine Expeditionary forces that can maneuver from the sea and sustain its C4I and life support systems in place; the only liquid fuel needed will be for mobility systems which will be more energy efficient than systems are today. [2]

Executive Order 13423 of January 2007 mandates the consumption of greater than 50 percent of renewable energy from new renewable sources and to implement renewable energy generation projects on agency property [3].

This thesis aims to design a vibrational energy harvesting MEMS device that will harness waste vibrational energy to produce usable power for naval applications. Ideally, MEMS microstructures will produce a maximum power output at a resonant frequency [4] equal to 3600 rpm, the operating frequency of the LM2500 Gas Turbine Engine [5], which is found in many midsize naval vessels. While this technology will not significantly limit the need for petroleum-based fuels, it can add to the portfolio of energy production options for military use in small electronics such as sensors. The vibrational energy harvester can have significant value in operations that limit access to electric generators. With slight modification, this technology may be optimized for other sea-

going, expeditionary platforms and ashore facilities. The development and widespread use of vibrational harvesting MEMS would aid the effort to meet each of these goals in the Department of the Navy, increasing current energy efficiencies, ultimately reducing the dependence on petroleum-based electricity, increasing the Department of the Navy's energy security.

B.   SCOPE OF THESIS

This thesis investigates the power output of a device whose microfabrication steps are aligned with the standard MEMS microfabrication techniques and which is designed to have fundamental resonant frequency of 60 Hz, matching that of a 3600 rpm motor. An optimal MEMS design is modeled and simulated with the COMSOL Multiphysics program. An in-depth analysis of the fabrication process needed to build the device is studied in order to produce a set of microfabrication steps required to produce an actual device. Aluminum nitride (AlN) is utilized due to its piezoelectric properties [6]. To improve the model, a set of AlN piezoelectric and electrical properties are required. We characterize the lattice structure of the piezoelectric material by means of x-ray diffraction and scanning electron microscopy [6]. The four-point contact probe device in the NPS clean room is used to determine the electrical properties of deposited AlN. A working prototype of the COMSOL Multiphysics model is obtained by sending our MEMS Pro designs to a MEMS fabrication company (MEMSCap) [7]. Our group has been selected as a super-user for free access to help characterize their new piezoelectric device microfabrication process. This thesis looks at optimizing the device structure as well as the fabrication process needed to build it, with the end goal of producing the MEMS waste vibrational energy harvesting device. This research will lay the groundwork for building deployable prototype vibrational waste-energy harvesters, featuring arrays of multitude of optimized devices for improved output.

II. PHYSICS WITHIN THE DESIGN

A. MICROELECTROMECHANICAL SYSTEMS

MicroElectroMechanical Systems (MEMS) are structures or mechanisms with one or more geometrical dimensions on the order of one to hundreds of micrometers in size and comprise small electro-mechanical systems that are produced utilizing microfabrication techniques. Miniaturized structures, sensors, and actuators make up MEMS, allowing the devices to convert one form of energy into another. In recent decades, MEMS researchers and developers have micromachined devices that outperform macroscale counterparts while leveraging the cost effectiveness of batch fabrication used in the microchip industry [8].

B. PIEZOELECTRIC EFFECT

Vibrational energy imparted on a MEMS can be converted to electrical energy via the piezoelectric effect. The piezoelectric effect is a phenomenon where charge within a material is separated as a result of an applied mechanical strain. This effect, discovered in the nineteenth century, can produce a 1000 V/cm field from a 10^{-7} strain in certain piezoelectric materials. The piezoelectric effect is strongly orientation-dependent and occurs solely in non-centrosymmetric crystals [9]. Qualitatively, in a piezoelectric crystal, the equations describing the mechanical and electrical behavior can be rendered as:

$$\delta = \sigma/Y + dE$$
$$D = d\sigma + \varepsilon E$$

(1)

where δ is the mechanical strain, σ is the mechanical stress, Y is the Young's modulus, d is the piezoelectric strain coefficient, E is the electric field, D is the electrical displacement (charge density), and ε is the dielectric constant. The piezoelectric coupling term (d) quantifies the amount of power generation from the harnessed vibrations [10]. In general, strain, stress, piezoelectric strain, and dielectric coupling are tensors. The piezoelectric stress is a tensor of rank 3 while the others are rank-2 tensors. Piezoelectric materials such as aluminum nitride (AlN) and lead zirconate titanate (PZT) possess high

coupling between the electrical and mechanical domains [11]. The output voltage, V, is related to the z-component of the electrical displacement D_3, by:

$$V = \frac{D_3 t}{\varepsilon}$$

(2)

where t is the thickness of the piezoelectric material in the z-direction. The only term utilized in the final equation occurs in the principal polarization direction, since contributions from components in other directions have negligible effects for piezoelectric materials polarized in the z-direction [9].

C.   CURRENT GENERATION

When no mechanical stress is present upon piezoelectric materials, it is considered electrically stable in a neutral electric state. When a stress or strain is applied to a piezoelectric material, its electrons align to the polar surfaces of the material, dependent upon the piezoelectric material crystal orientation. The positioning of the induced polarization depends on the direction of the mechanical stress. An applied stress in one direction may give rise to an induced polarization in other crystal directions [12], as discussed in Chapter III Section B. This separation of charge can be harnessed for electrical current through circuitry. Due to the rapid rate of charge leakage that occurs in strained piezoelectric materials, an oscillating voltage is necessary to harness current for useful power output. This oscillating voltage is generated by the oscillating strain imparted on the piezoelectric energy harvester by the means of mechanical vibration [8].

D.   VIBRATIONAL MODES AND DEVICE CONFIGURATION

A MEMS device has many resonant modes of vibration, with each subsequent mode occurring at a higher frequency than the last. Energy harvesters are typically designed to operate in the first resonant mode, since it typically has the lowest resonant frequency and highest overall amplitude, resulting in the highest electrical energy output [10]. In order to fabricate a MEMS device with a low resonant frequency, the spring constant of the supporting beams must be decreased, while the oscillating mass should be increased. While many MEMS devices utilize a fixed-free cantilever beam structure for

4

its small spring constant [13], this thesis utilizes a fixed-fixed bridge structure in order to harness the potential difference created when mechanical load is applied in the z-direction to the piezoelectric material (see Chapter IV, Section B). In order to reduce the resonant frequency of the fixed-fixed bridge design, this MEMS device incorporates multifold legs representing springs with a lower spring constant and a large pad mass. When the piezoelectric MEMS energy-harvesting device is subject to vibrations in the vertical direction, the structure will deform in accordance to the external force. A lower spring constant will lead to a larger deflection for the same force, yielding more mechanical stress and consequently a higher output voltage [10].

THIS PAGE INTENTIONALLY LEFT BLANK

III.   MATERIALS SELECTION AND ANALYSIS

One of the most important aspects to many MEMS applications is the selection of materials. The response to the physics noted earlier is dependent on both the operating environment and the materials utilized.

A.   PIEZOELECTRIC MATERIALS

The materials selection logically followed the criteria set forth in the physics and concepts described earlier. The piezoelectric material, as well as the device as a whole, must be capable of being microfabricated with current MEMS manufacturing techniques. The material must also have adequate piezoelectric properties for high efficiencies of energy conversion.

1.   Lead Zirconium Titanate (PZT)

PZT has been tested for many piezoelectric generators due to its large piezoelectric strain coefficient and dielectric constant, yielding higher power for a given force when compared to other piezoelectric materials [13]. However, PZT is considered a brittle material that cannot withstand large mechanical stress without fracturing [11]. Since a goal of this thesis is to design an energy harvesting MEMS device with a low resonant frequency, PZT was not ultimately chosen as a piezoelectric material due to possible mechanical fatigue.

2.   Aluminum Nitride (AlN)

AlN was the piezoelectric material chosen for development of the MEMS energy-harvesting device. Although PZT is used more prevalently due to its higher piezoelectric coefficient and dielectric constant, AlN has advantages in metal deposition techniques and compatibility with standard complementary metal-oxide-semiconductor (CMOS) fabrication technology [13]. AlN has a large band gap (6 eV) made of a wurtzite crystal structure with a large resistivity and is perfectly compatible with current silicon technology [8]. Many methods for growth of AlN exist including chemical vapor deposition (CVD), molecular beam epitaxy, ion beam nitridation, laser-ablation, and

reactive sputtering [9]. Additionally, the successful growth of AlN for laboratory purposes is facilitated by the fact that sputtered AlN maintains its piezoelectric properties with growth up to 10° offset from normal without losing the functionality of the piezoelectric layer [10]. AlN, which demonstrates moderately good piezoelectric properties, has been shown to have no deviation in its piezoelectric constants up to 300℃ and only slight alteration is expected up to a temperature of 1150℃ [10]. In summary, AlN is a highly stable, non-reactive piezoelectric material that exhibits the desired properties for the vibrational energy harvesting MEMS device.

B.   PIEZOELECTRIC MATERIAL ORIENTATION

Piezoelectric materials have built-in polarization, resulting in different material responses based on directional stress. As seen in Figure 1, piezoelectric materials have two primary modes of electromechanical coupling, the 33 mode and the 31 mode of coupling. Three principal axes, termed 1, 2, and 3 corresponding to x, y, and z, are used to describe direction when referring to piezoelectric materials. The polar, or 3 axis, is taken parallel to the direction of built-in polarization within the material, which is established during deposition [14]. In most MEMS applications, this is the direction perpendicular to the substrate. In the 33 mode, the electric field is produced parallel to the applied mechanical stress, while the electric field is produced orthogonally to the applied mechanical stress in the 31 mode. While the piezoelectric strain coefficient is higher in the 33 mode when compared to the 31 mode, the advantage is negated when design complexity is taken into account [13]. Operating in the 31 mode allows for the use thin bending elements, resulting in larger strains being exploited from smaller input forces, lowering the resonant frequency of the energy harvesting MEMS device [10].
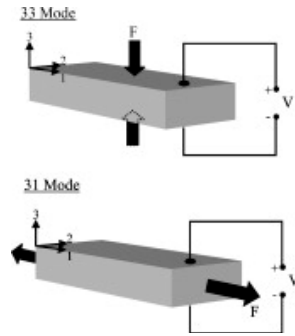
Figure 1.   Piezoelectric material modes of operation. From [10].

The microscopic mechanism for piezoelectricity is the displacement of ionic charges within a crystal, which creates polarization. Crystal orientation in relation to mechanical stress can impact the voltage output created piezoelectrically. In a comparison of AlN with a c-axis orientation and a (101) orientation, films with (101) orientation show lower effective longitudinal piezoelectric coefficients [6]. Fabrication efforts in this thesis are designed to deposit thin film AlN with a high c-axis orientation, with device operation in the 31 mode. Figure 2 shows how the voltage for the devices discussed in this thesis are oriented when compared to the applied strain, with resultant operation in the 31 mode. Figure 2a) shows the magnitude of y component of strain (highest on the top of the film) parallel to the y direction. Figure 2b) shows the electric field parallel to the z direction.
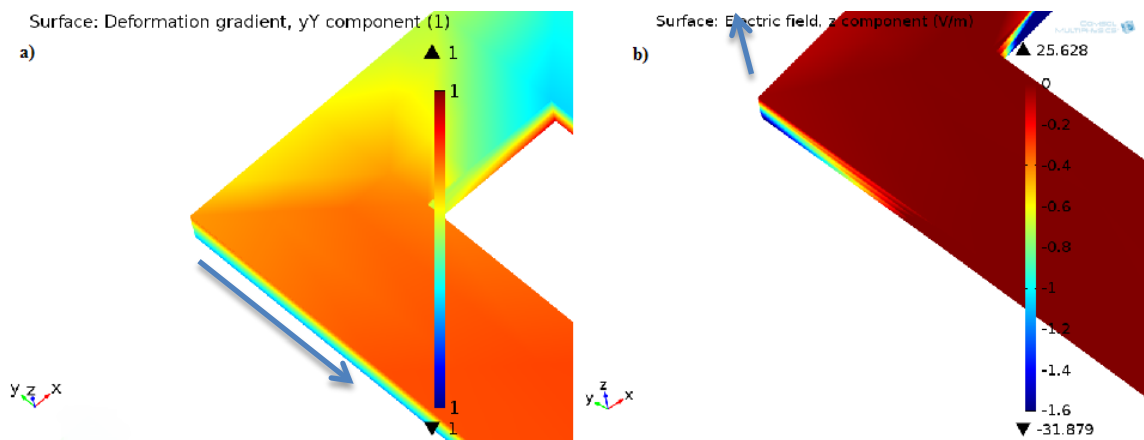
Figure 2.   31-mode operation a) x-y oriented strain due to static force b) z oriented electric field due to static force.

9

C.   SUBSTRATE

As micromachining technology developed, silicon was readily accessible and remains the substrate of choice for MEMS fabrication [8]. The devices in this thesis will be fabricated on Silicon on Oxide (SOI) wafers, chosen for the buried layer of SiO_2 that serves as a sacrificial layer and aids in fabrication of suspended mechanical structures. Most SOI wafers are comprised of three layers including a base of about 400–600 µm single-crystalline silicon, underneath a 0.5–10 µm silicon oxide layer, followed by a top layer of 1–20 µm silicon. The specific thicknesses of the SOI wafers used in this research vary and will be described in detail in the fabrication section of this thesis.

IV. DESIGN

A. GENERAL DIMENSIONS

Current methods of microfabrication offer a standard thin film deposition of MEMS materials between 1–10 microns on substrate. As mentioned previously, the scope of this thesis is to achieve a resonant frequency of 60 Hz, done so with a device that utilizes a small spring constant. If k is the spring constant,

$$k = \frac{Ewt^3}{4l^3} , \tag{3}$$

E is the Young's modulus, w is beam width, t is beam thickness, and l is beam length. Minimizing the thickness to length ratio of the energy harvesting MEMS device will allow a low spring constant objective to be achieved. A piezoelectric cantilever beam that is very long and very thin would produce the maximum voltage. Based on microfabrication constraints and structural integrity concerns, beam length and thickness need to conform to certain constraints. In order to maximize effective beam length, the designed MEMS device incorporates multifold arms which simulate longer beam length.

1. Design 1: Naval Postgraduate School Fabrication

The preliminary energy harvesting MEMS devices that are being fabricated at NPS, with the AlN being deposited at OEM Group [15], feature a large central pad, serving as a proof mass, with multifold arms that are fixed at the ends, mirroring a design initially used for MEMS solar energy harvesting [9]. The purpose of these devices is to understand the fabrication steps necessary to create a future device that will have an eigenfrequency of 60 Hz. These preliminary devices, that include multifold devices and simple fixed-fixed bridges, will also aid in verifying and fine-tuning the models simulated in COMSOL Multiphysics.

The structures are fabricated on an undoped SOI wafer of the following dimensions:

- Silicon thickness: 2±0.05µm

- Oxide thickness: 2±0.05µm

- Substrate thickness: 350±5µm

Figure 3 is a graphic from the MEMSPro design program used to create a photolithographic mask for the energy harvester fabrication. The masks shown produce eight dies, each with a varied design of the piezoelectric energy harvester.
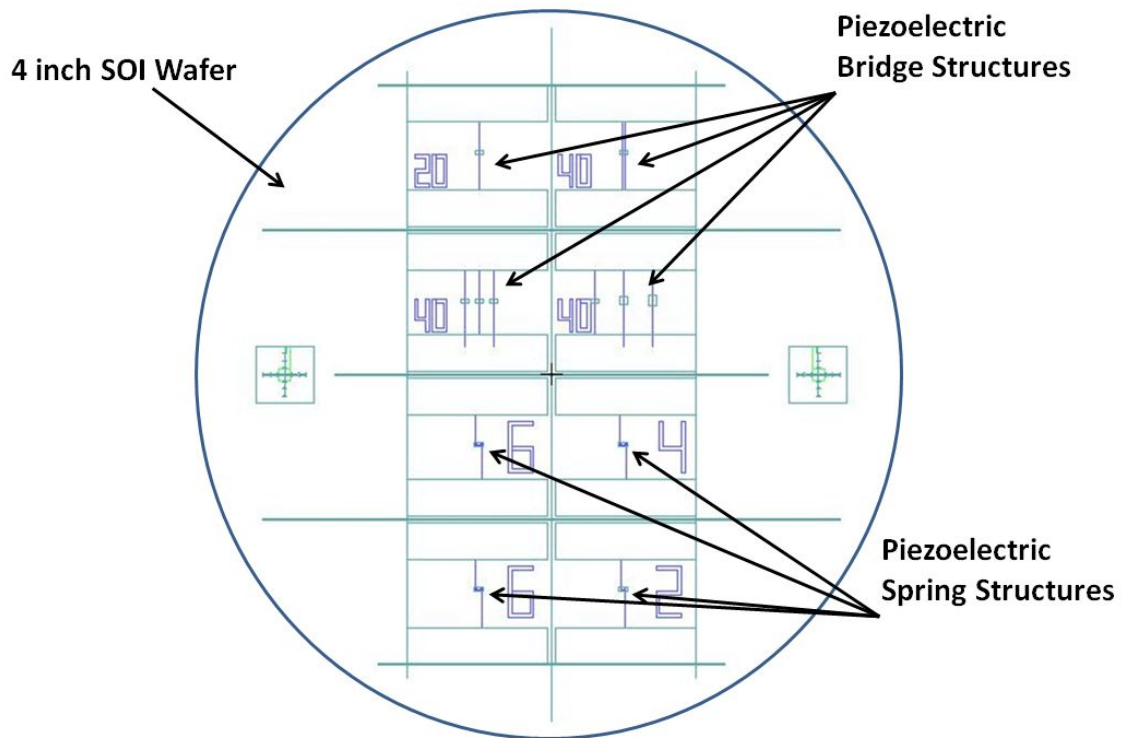
Figure 3.   MEMSPro graphic for the mask used in the NPS fabrication, with structural annotation.

The top four dies in this mask are bridge structures of varied width, with trenches of various sizes beneath this midsection of each bridge, to release the structure and allow for free mechanical motion. These bridges are there as they are simpler to simulate and

could help use finite element modeling to extract piezoelectric properties of the material. Figure 4 is a close-up of the top left die, which is a 20 micron bridge on top of a trench 1000 by 500 microns squared.
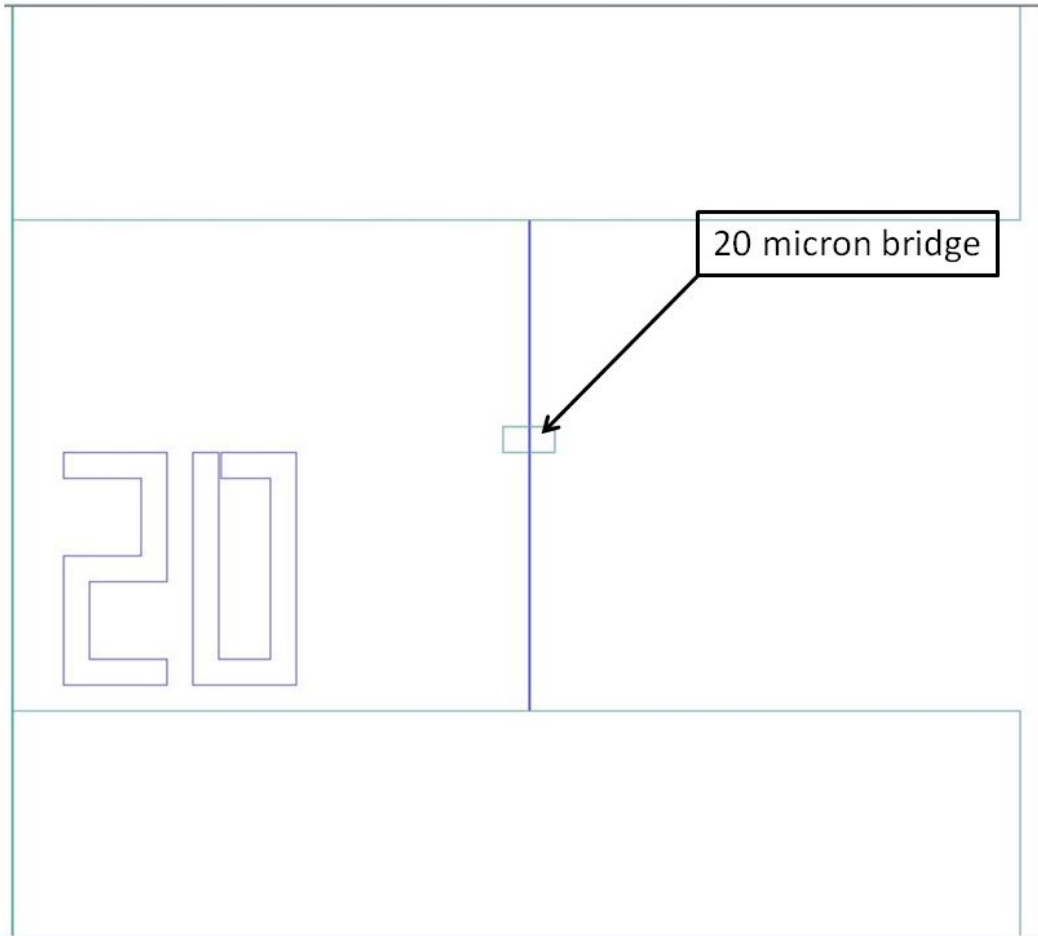
Figure 4.   MEMSPro graphic of the mask for a 20-micron bridge.

The lower 4 dies in Figure 3 are the "spring" design emphasized in the COMSOL modeling of this thesis. These dies vary by the number of legs on each structure, denoted by the number on each die. Figure 5 is a close of up the bottom left dies (as they are identical), which are six legged structures. Figure 5 also illustrates the structural function of each mask in the MEMSPro graphic.   Figure 6 is a 3D graphic, developed in

MEMSPro, of the same structure. This structure is hypothesized to be the most successful piezoelectric energy harvester from this fabrication series.
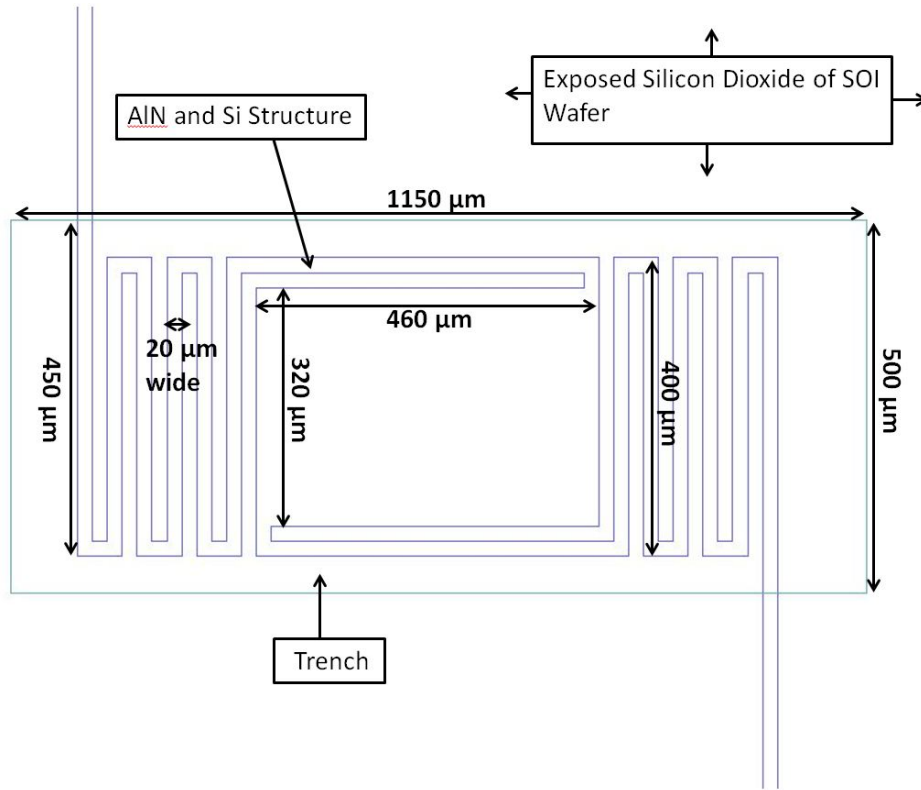
Figure 5. MEMSPro graphic of the mask for a 6-legged piezoelectric energy harvester, annotated with structure notes and dimensions.

14
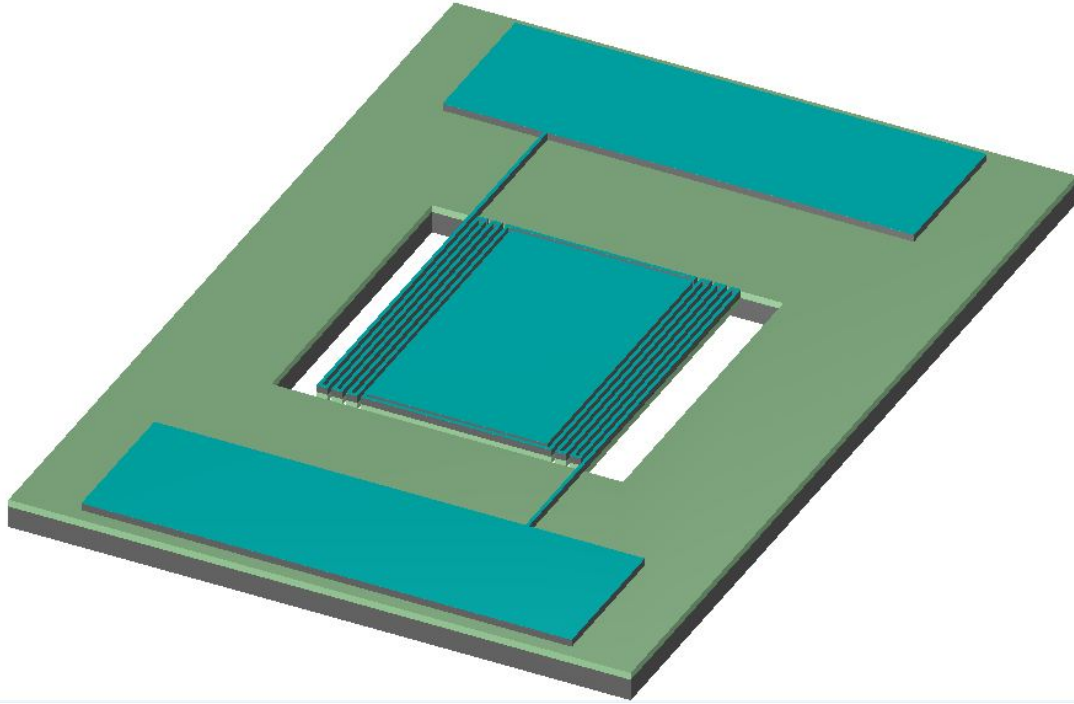
Figure 6.   MEMSPro graphic of the final piezoelectric energy harvester after fabrication. AlN is in blue, Si is grey and buried oxide from the SOI wafer is green.

2.   Design 2: PiezoMUMPS Fabrication

PiezoMUMPS allows for 4.5 mm by 4.5 mm of device area.   A lower eigenfrequency will be achieved with a larger device, resulting in the entire available area being utilized by one device for this initial trial. COMSOL Multiphysics, as described in the following chapter, was used to fine-tune dimensions to match the 60 Hz resonant frequency.

MEMSPro v. 8.0 software was used to design the specific masks to be used in each phase of fabrication. MEMSPro was also used to specify the fabrication process for both the design fabricated by the PiezoMUMPS program and the design fabricated by NPS/ORNL and MEMSCAP Company.

There were two designs submitted for fabrication, a high frequency model and a low frequency model. The high frequency model, in Figures 7, 8 and 10, is a 6-legged AlN piezoelectric energy harvester. The spring structure is fabricated on an n-type SOI wafer of the follow dimensions:

- Silicon thickness: $10\pm1\mu m$
- Oxide thickness: $1\pm0.05\mu m$
- Substrate thickness: $400\pm5\mu m$

Looking from the top, the exposed silicon substrate of the SOI wafer is shown in red in Figure 7. The AlN spring is shown in blue. The AlN spring is free to oscillate over a trench that tunnels through the entirety of the wafer. Attached to the outer legs of the AlN spring are two metal pads, for the purpose of attaching other devices to the piezoelectric energy harvester to enable the measurement of power produced by the vibrational energy harvesting MEMS device. These pads are two layers. The first layer is 200 nm of PADOXIDE, which is a thermal oxide used to electrically isolate the upper pad layer from the SOI wafer. The second layer is 1020 nm of PADMETAL, which is a metal stack of 20 nm of chrome and 1000 nm of aluminum [16]. As found through COMSOL modeling, the expected eigenfrequency of the high frequency PEH is approximately 60 Hz, as shown in chapter IV.
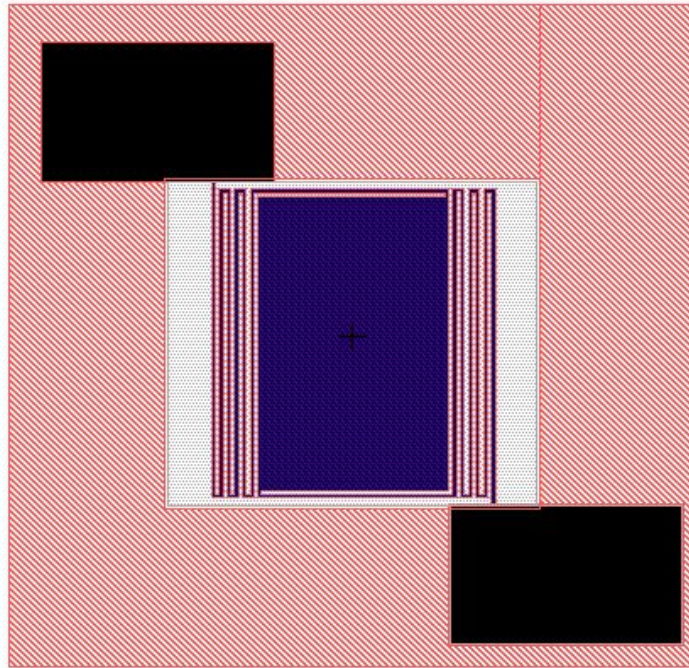
Figure 7.   Mask design of high frequency, 60 Hz model, MEMSPro v. 8.0.
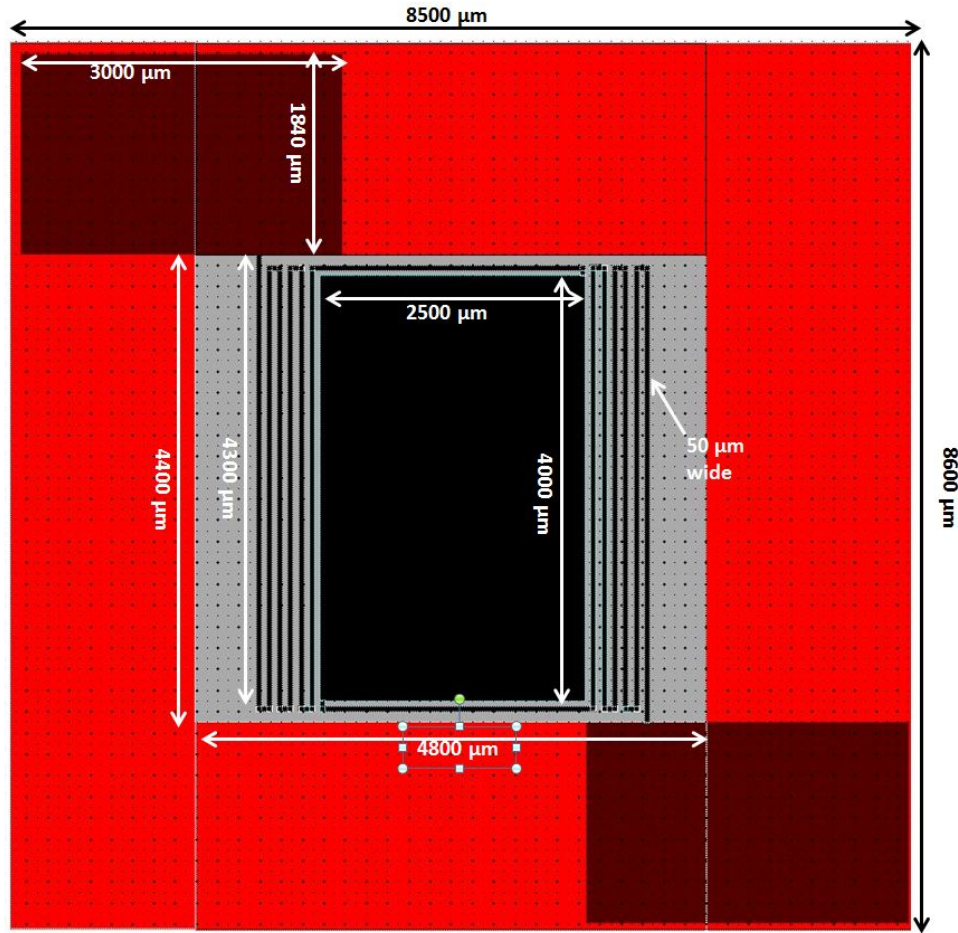
Figure 8.   Mask design of high frequency, 60 Hz model, MEMSPro v. 8.0, annotated with design dimensions.

The low frequency design, shown in Figures 9 and 11, varies only slightly from the high frequency model. The dimensions and materials of the vibrational energy harvesting MEMS device are identical to those used in the high frequency model, except for the addition of 1020 nm of PADMETAL to the center area of the AlN spring. The added weight of the spring should decrease the eigenfrequency, as shown in Equation 3. As found through COMSOL modeling, the expected eigenfrequency of the low frequency PEH is approximately 56 Hz, as shown in Chapter IV.
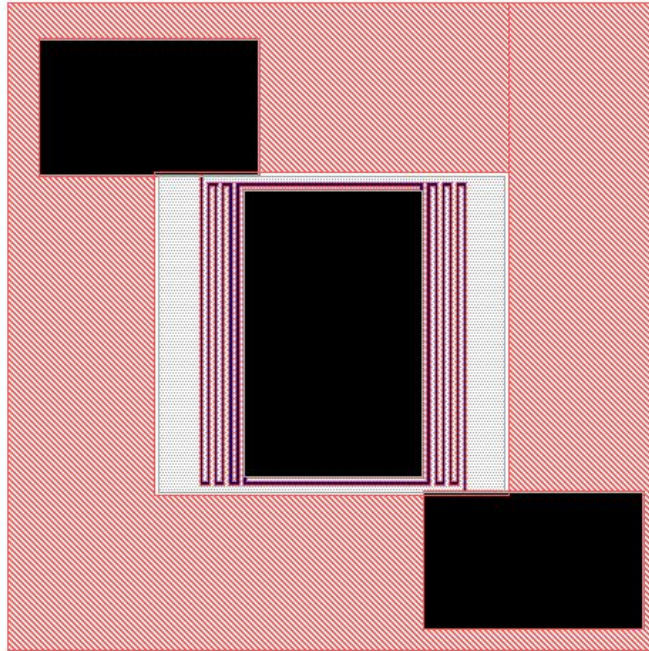
Figure 9.   Mask design of low frequency, 56 Hz model, MEMSPro v. 8.0.
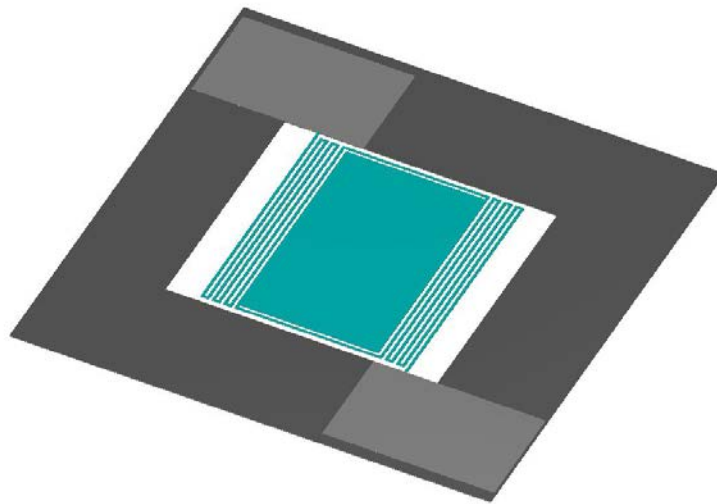
Figure 10.   Top-down profile of high frequency, 60 Hz model. The blue green area
indicates an AlN surface. The light grey area indicates a PADMETAL
surface. The dark grey area indicates a Si surface.
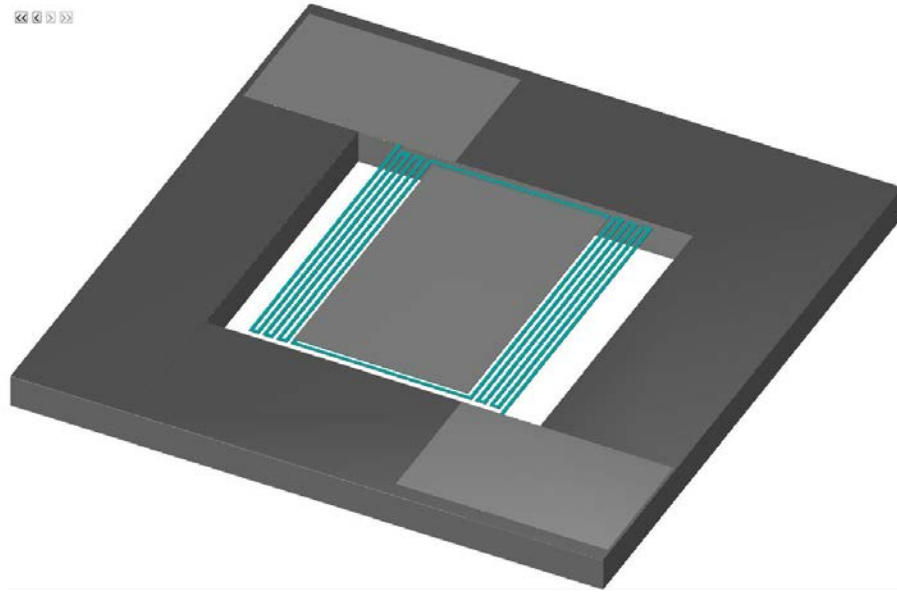
Figure 11.　　Top-down profile of low frequency, 56 Hz model.

V. COMSOL MULTIPHYSICS MODELING

COMSOL Multiphysics finite element modeling software was used to optimize the size and shape of the energy harvesting MEMS in order to fabricate future devices. Two different models of the device were designed. The initial models were fabricated at Naval Postgraduate School, with certain fabrication steps performed by the OEM Group [15] , with the goal of developing the fabrication techniques of future models as well as verifying the finite element model by comparing model results with experimental measurements. The initial designs were designed for higher frequencies in order to utilize testing equipment at NPS, which is not as reliable at lower frequencies. The second model was fabricated, per our design, entirely in the PiezoMUMPS pilot program through MEMSCAP Inc., with the goal of obtaining a device closer to deployable sensors, with an eigenfrequency of 60 Hz. Resonant behavior was studied for all of devices; however, considering that the main application was to harvest vibrations at lower frequencies, this thesis studied the mechanical response to vibrations and power output only for PiezoMUMPS microfabricated devices.

A. EIGENFREQUENCY

Using the piezoelectric physics model within COMSOL, the eigenfrequencies of the MEMS energy harvesting devices were obtained.

1. Naval Postgraduate School Device Modeling

An extruded view of the NPS design with 6 multifold arms can be seen in Figure 12. The dimensions of the NPS devices, listed in Table 1, were used to build and simulate the structures in COMSOL. The frequencies of the first four modes for each multifold device can be seen in Table 1. A visual representation of the deformation of the first four eigenfrequency modes for each multifold device can be seen in Figures 13 through 15. For future models, the design with 6 multifold arms on each side of the central pad was chosen over designs with 2 and 4 multifold arms on each side of the central pad in order to achieve a lower device eigenfrequency.

21
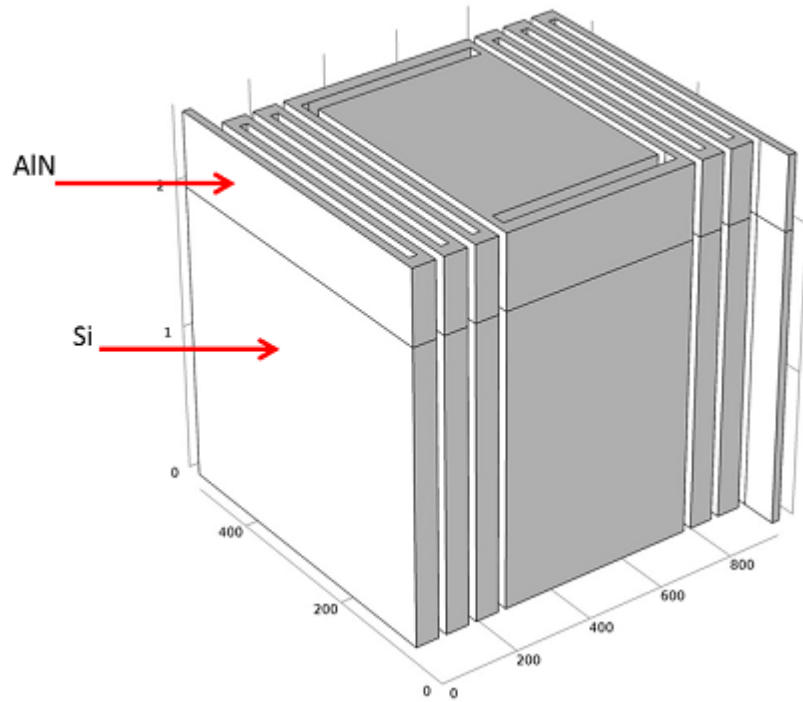
Figure 12.   Energy harvesting COMSOL 6-leg NPS fabricated MEMS.

Device	Device area	1st order eigenfrequency	2nd order eigenfrequency	3rd order eigenfrequency	4th order eigenfrequency
2-leg	620 μm x 500 μm	2505.47 Hz	4167.33 Hz	5532.73 Hz	14251.35 Hz
4-leg	780 μm x 500 μm	2030.37 Hz	3366.86 Hz	4865.44 Hz	9635.60 Hz
6-leg	940 μm x 500 μm	1701.07 Hz	2784.91 Hz	4527.04 Hz	4538.98 Hz

Table 1.   Areas and eigenfrequencies of preliminary NPS fabricated MEMS devices.
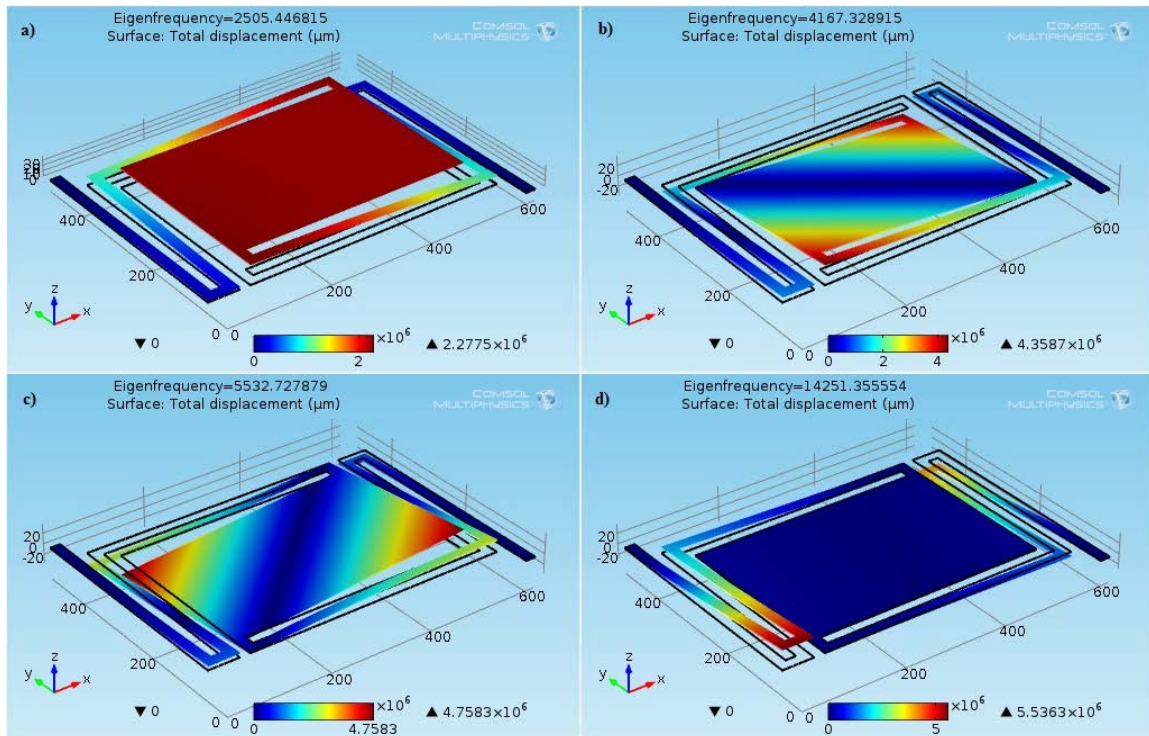
Figure 13.   a) 1st order b) 2nd order c) 3rd order d) 4th order eigenfrequency of 2-leg NPS energy harvesting MEMS device.
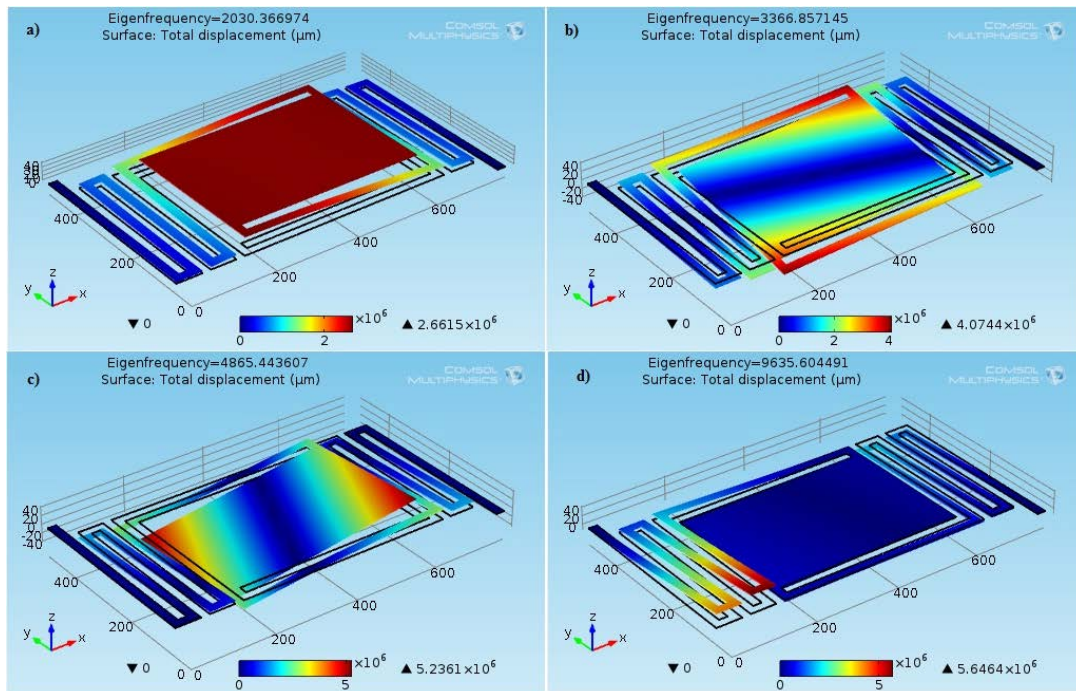
Figure 14.   a) 1st order b) 2nd order c) 3rd order d) 4th order eigenfrequency of 4-leg NPS energy harvesting MEMS device.
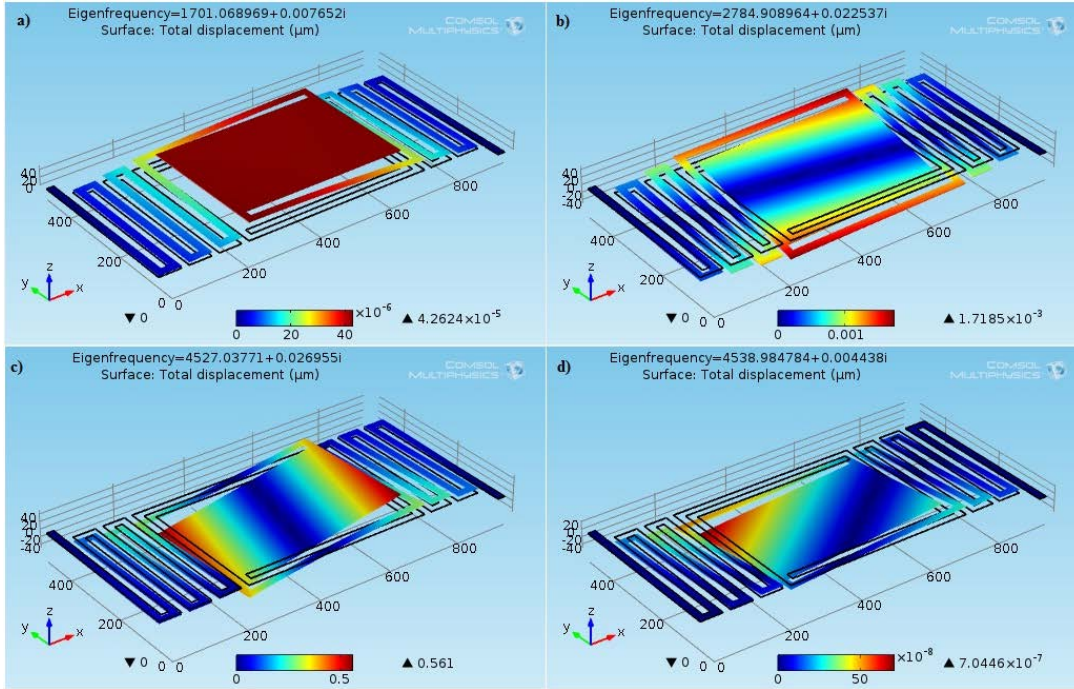
Figure 15.   a) 1st order b) 2nd order c) 3rd order d) 4th order eigenfrequency of 6-leg NPS energy harvesting MEMS device.

2.   SOIMUMPS Device Modeling

In order to achieve a device eigenfrequency of 60 Hz, the design used for the SOIMUMPS device required a larger overall size and different aspect ratio.   The multifold arms were made longer in order to reduce the effective spring constant and the central pad was made larger in terms of both length and width in order to increase the mass.   These changes ensured that the resonant frequency, proportional to $\sqrt{k/m}$, was significantly lower than the devices produced at NPS.   The device consisted of silicon and aluminum nitride layers as shown in Figure 16. The deformation of the first four eigenfrequency modes of the roughly 4.5 mm by 4.5 mm SOIMUMPS device are visually represented in Figure 17.
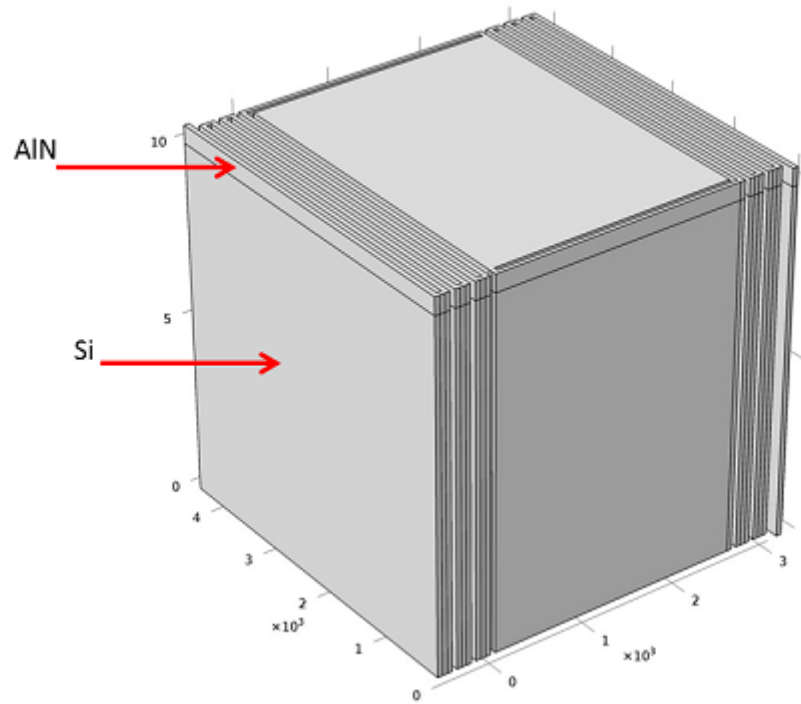
Figure 16.   Energy harvesting PiezoMUMPS COMSOL 6-leg MEMS device.
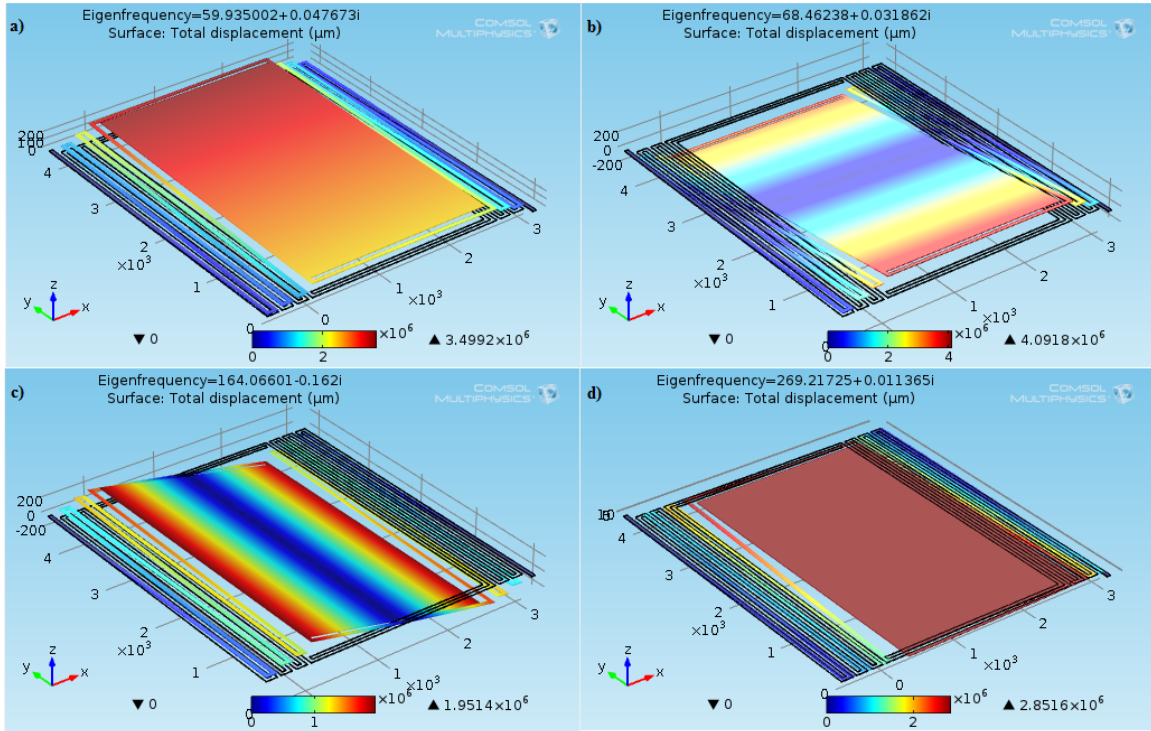
Figure 17.   a) 1st order b) 2nd order c) 3rd order d) 4th order eigenfrequency of
SOIMUMPS fabricated energy harvesting MEMS device.

In order to achieve an even lower eigenfrequency, and since the PiezoMUMPS process provided the option, a 1 micron thick aluminum (Al) block was added to the middle pad and simulated in COMSOL. An extruded view of the MEMS device with 10 microns of Si substrate, 0.5 microns of piezoelectric AlN, and 1 micron of Al pad metal is shown in Figure 18. The first four eigenfrequency modes of the device, along with the original 6-leg PiezoMUMPS device can be seen in Table 2. The deformation of the first four eigenfrequency modes of the PiezoMUMPS experimental COMSOL 6-leg MEMS device with Al pad can be seen in Figure 19. Since the model with the added Al block only achieved a slightly better eigenfrequency result when compared to the PiezoMUMPS device without, further COMSOL modeling in this thesis is performed on the latter. If future work requires the device to operate at a lower eigenfrequency, more simulation with the Al block on the center pad may become a viable option.
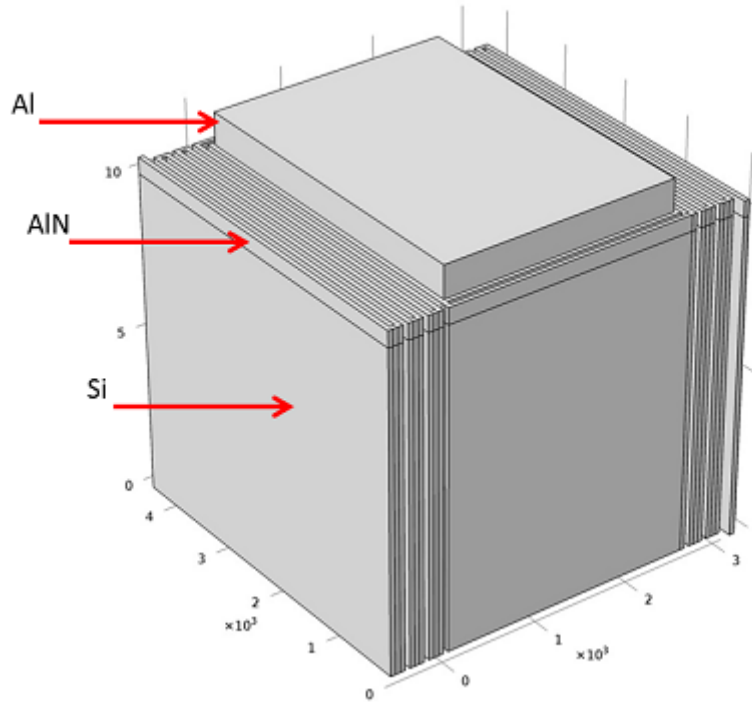
Figure 18.   Energy harvesting PiezoMUMPS COMSOL 6-leg MEMS device with eigenfrequency lowering Al block.

Device	1st order eigenfrequency	2nd order eigenfrequency	3rd order eigenfrequency	4th order eigenfrequency
SOIMUMPS 6-leg	59.94 Hz	68.46 Hz	164.07 Hz	269.22 Hz
SOIMUMPS 6-leg with Al pad	56.13 Hz	63.69 Hz	158.11 Hz	259.38 Hz

Table 2.   Eigenfrequencies of PiezoMUMPS fabricated MEMS device and experimental COMSOL 6-leg MEMS device with Al pad.
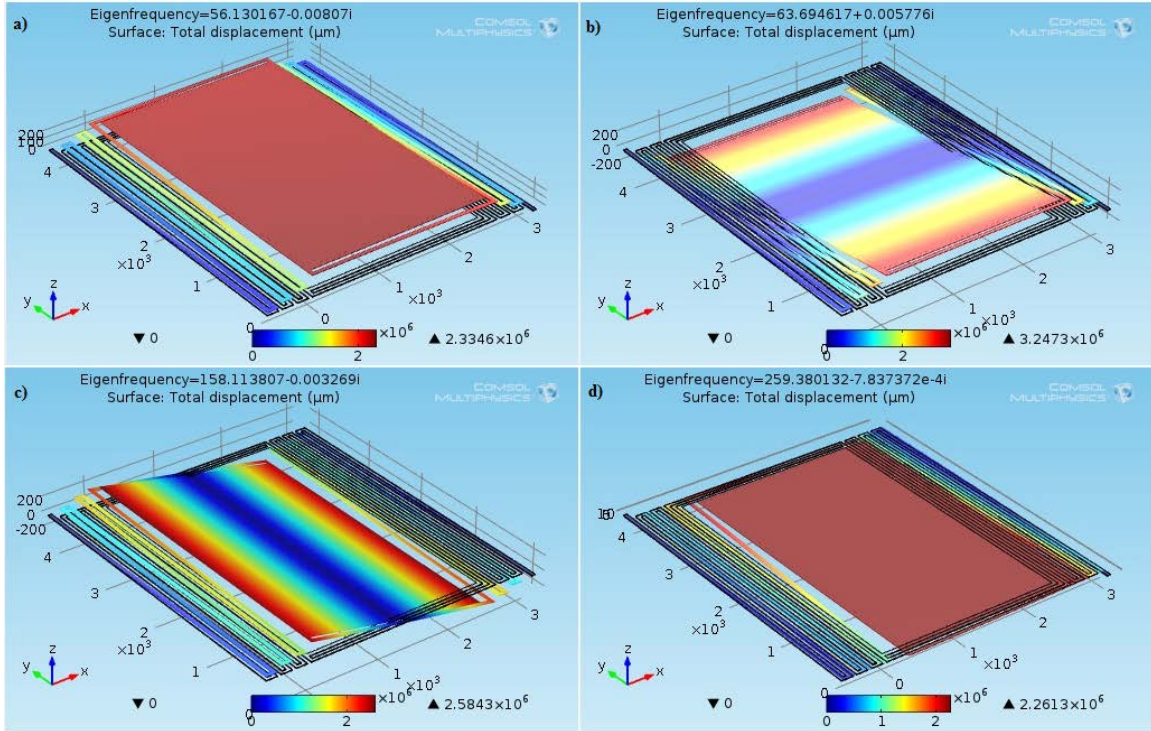
Figure 19.   a) 1st order b) 2nd order c) 3rd order d) 4th order eigenfrequency of experimental COMSOL 6-leg MEMS device with Al pad.

B.   TIME-DEPENDENT DISPLACEMENT

In order to analyze the temporal response due to a periodic vibrational actuation, and calculate the power output of the energy harvesting MEMS device, a time-dependent study was modeled in COMSOL.   The resonant motion of the MEMS device was modeled in COMSOL by simulating a shaker that is to be used for experimental measurements. This was achieved by providing prescribed displacement to the surfaces where the device is attached to the substrate and displacing them by 0.1 mm using a 60 Hz sine function oriented in the z direction. The same surfaces were constrained in x and y directions. The study covered 200 ms and ensured a steady state was achieved. Figure 20 shows the displacement of the main pad (proof mass) relative to the fixed ends of the MEMS device when running a time-dependent solution from 0-0.2 seconds at 0.5 ms time-steps.   The steady state, per the model, is achieved after only a few periods. However, it should be noted that the damping coefficients used were arbitrary and that the correct values will be obtained once the first of the models is experimentally tested.

28
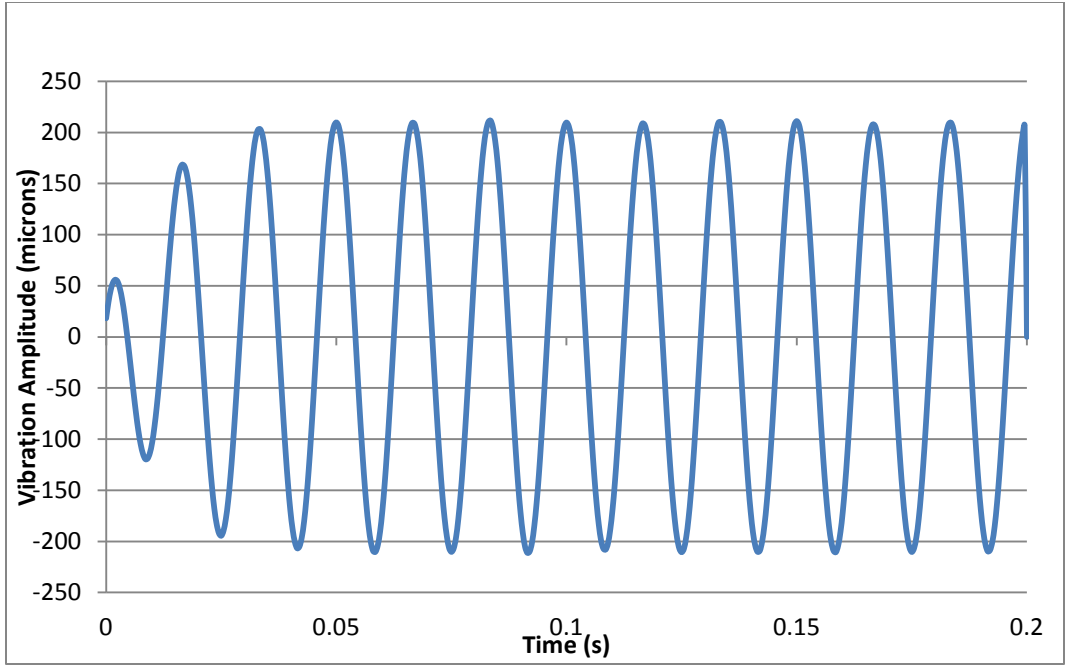
Figure 20.   Time-dependent displacement of PiezoMUMPS center pad with fixed ends driven at 0.1 mm, 60 Hz resonant frequency. Note that steady state is achieved after 0.05 s.

C.   VOLTAGE GENERATION

The piezoelectric physics model within COMSOL was also used to simulate the voltage created by the MEMS device when driven at resonant frequency as shown in Figure 21. Driving the MEMS device close to its natural frequency allows for a high energy conversion efficiency due to the large ratio between the electromechanical coupling coefficient and the mechanical damping ratio [17]. In order to view the voltage during resonance, an initial time period of 200 ms was simulated in COMSOL to get the device into resonant motion. The difference in electric potential between the top and bottom piezoelectric AlN layers, in accordance with the 31 mode of operation discussed earlier, with no attached electrical load, is estimated to be 2 mV as seen in Figure 21.
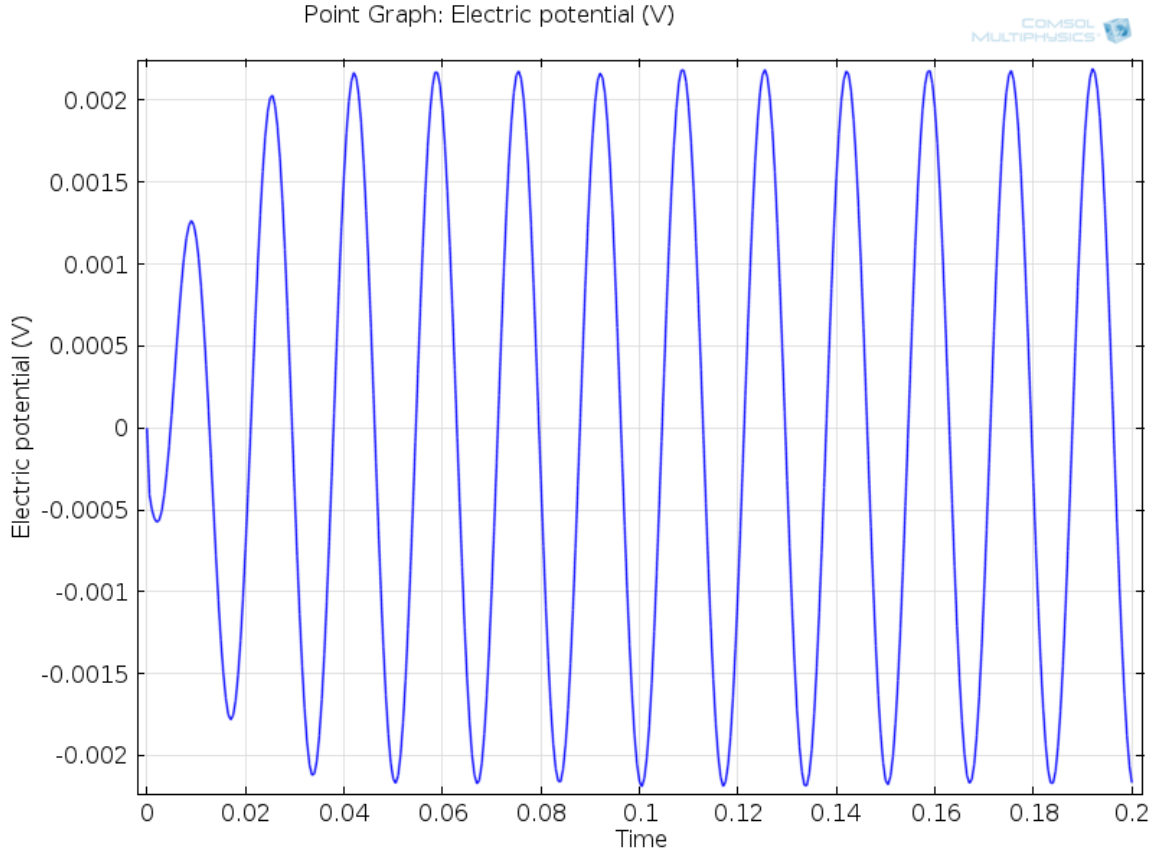
Figure 21.   Open-ended voltage plot of PiezoMUMPS MEMS device driven at a resonant frequency of 60 Hz.

D.   CURRENT AND POWER GENERATION

Utilizing the COMSOL electrical circuit study module allows for simulation of a resistor connected between the top and bottom surfaces of the piezoelectric material. The current produced by the energy harvesting MEMS device, when connected to an electrical load, was used to simulate the total electrical power output of the MEMS device. From Ohm's Law, $P = V \cdot I$, the electrical power, P, produced by the device, when driven at resonance, can be determined and plotted in COMSOL. Figure 22 shows the time-dependent electrical power dissipated across 1 kΩ, 1 MΩ and 10 MΩ resistors, produced by the device when anchoring ends of the MEMS device are actuated at 0.1 mm displacement, 60 Hz resonant frequency. From Figure 22, it is apparent that the output power is dependent on the impedance of the load. Of the three resistances, the 1 MΩ resistor dissipates the most electrical power when the shaker device is displaced by 0.1

mm at the resonant frequency of the MEMS device, 60 Hz. Figure 23 shows that in simulations of vibrations of larger amplitudes, the power dissipated across a 1 MΩ resistor by the MEMS device exceeds 20 nW.
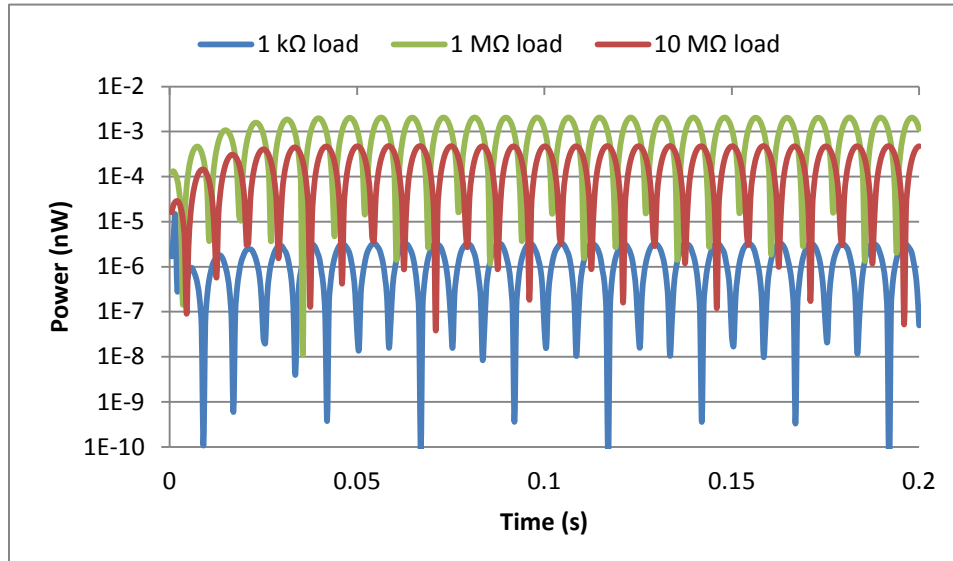
Figure 22.   Time-dependent electrical power output of PiezoMUMPS device across 1 kΩ, 1 MΩ and 10 MΩ resistors, driven at 0.1 mm displacement, 60 Hz resonant frequency.
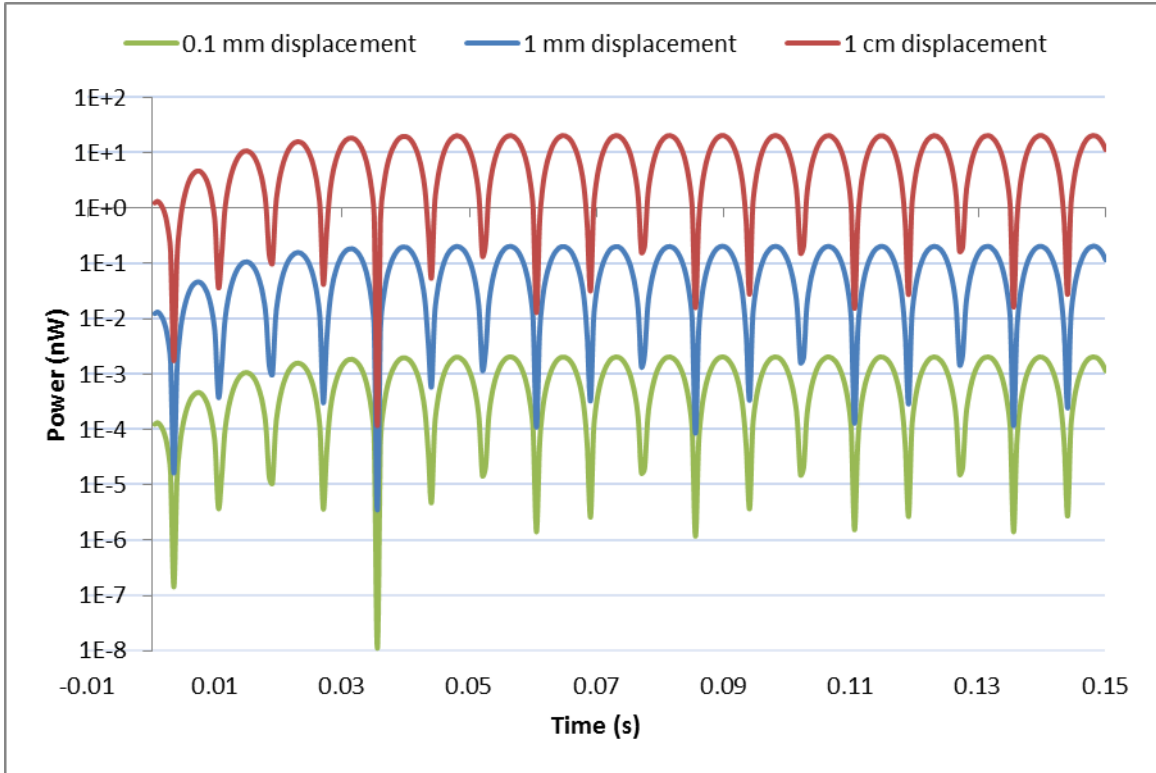
Figure 23.   Time-dependent electrical power output of PiezoMUMPS device across 1
MΩ resistor, driven at 1 cm displacement, 1mm displacement and 0.1 mm
displacement, at 60 Hz resonant frequency.

VI. MICROFABRICATION PROCESS

The following section will describe the processes by which each of the two MEMS designs are fabricated. We use two fabrication processes in this thesis; Process 1 contains the devices fabricated through the NPS Clean Room, and Process 2 contains the MEMS developed in the PiezoMUMPS program.

A. PROCESS 2: NAVAL POSTGRADUATE SCHOOL FABRICATION

The NPS fabrication top structure mask fabricates eight dies of varied MEMS designs on the same SOI wafer. Both piezoelectric bridges and PEH models of varied designs were fabricated, as shown in Chapter V.

1. Fabrication Steps

Fabrication begins with an SOI wafer, a section of which is shown in Figure 24a. Then, fabrication materials are deposited and etched in the following order:

1. AlN is deposited by AC powered S-gun magnetron for AlN reactive sputtering [18] [15], as shown in Figure 24b.

2. The wafer is primed by spinning the wafer at 3000RPM under several milliliters of MCC Primer, an organic solvent solution, to prepare the wafer for photoresist application [19].

3. 7 microns of SPR 220 photoresist are spin coated on the primed wafer at 3000 RPM for 40s. The wafer is then soft baked at 115°C for 90s.

4. Next, the photoresist was exposed under the mask described in Chapter V at between 220 and 520 Integra, with a print gap of 30 microns. The outcomes of both exposures at different Integra levels will be highlighted in Chapter VII.

5. The wafer rests for 30 minutes to allow for more solvent in the photoresist to evaporate. After at least 30 minutes, the wafer is post-exposure baked at 115°C for 90s.

6. Photoresist is developed for 3 minutes CD-26 developer, to remove exposed photoresist.

7. The AlN is isotropically etched, using 85% H3PO4 at 85°C for 60-80 seconds, as shown in Figure 24c.

8. Using the AlN as a mask, a reactive ion etch will remove the top layer of Si, as shown in Figure 24d.

9.   The top AlN and Si structures are protected by spinning the wafer surface with SPR 220-7, and then baking for four hours at 90°C [20].

10.   The bottom side of the wafer is primed, as it was in step 2. Next, it is spin coated with SPR 220-7 under the same conditions in step 3.

11.   The trench mask is aligned, using a backside aligner, which is available at Stanford University.

12.   Expose the wafer at 220 Integra, with a print gap of 30 microns. Develop for 3 minutes in CD-20. The result is shown in Figure 24e.

13.   Etch the trench through the bottom Si layer using deep reactive ion etcher.

14.   Remove the photoresist from the bottom layer, by soaking in acetone for 5 minutes and rinsing with isopropanol.

15.   Use reactive ion etch on the SiO_2 to complete the trench and release the energy harvesting structure, as shown in Figure 24f.
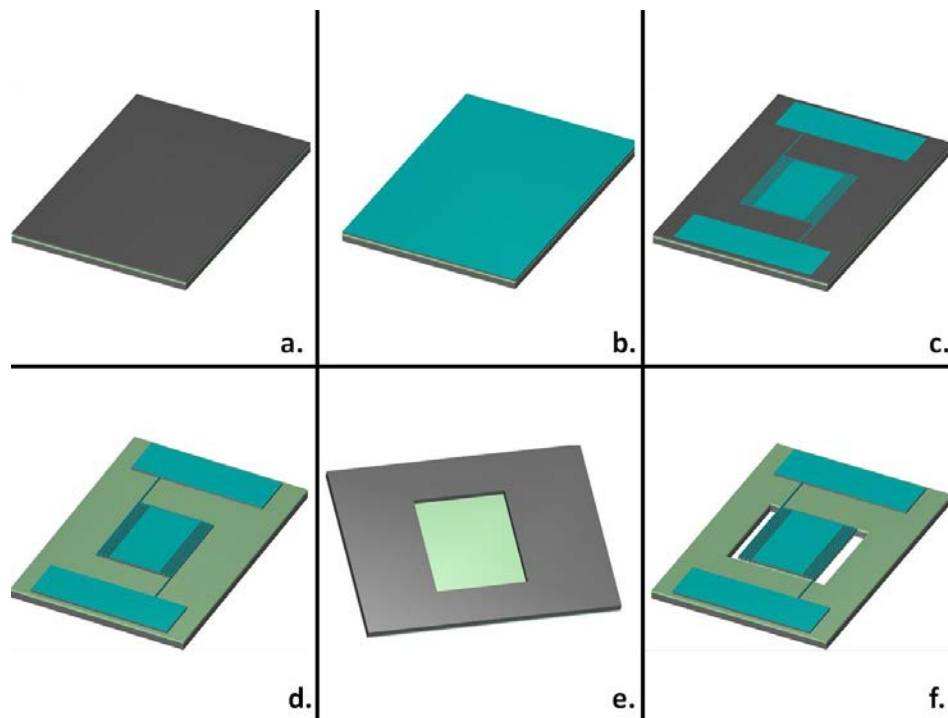
Figure 24.   The Naval Postgraduate School microfabrication. Silicon is shown in grey. SiO_2 is shown in green. AlN is shown in blue.

B. PROCESS 1: PIEZOMUMPS PROGRAM

The PiezoMUMPS program provides up to four dies of two different MEMS designs on the same SOI wafer. Both a low frequency model and a high frequency model were fabricated, as shown in Figures 10 and 11. These designs are similar, except a layer of PADMETAL remains on the center pad of the energy harvester spring in the low frequency model.

1. Fabrication Steps

The process used by MEMSCAP in the PiezoMUMPS program is outlined in detail in ref [16]. Fabrication begins, using an SOI wafer, shown in Figure 25a. Then, fabrication materials are deposited and etched in the following order:

1. Thermal oxide is deposited and etched, as shown in Figure 25b,c.

2. AlN oxide is deposited and etched, as shown in Figure 25d,e. This is reactively sputtered by dual cathode AC (40 kHz) [18]

3. PADMETAL, a metal stack of 20 nm chrome and 1000 nm aluminum, oxide is deposited and etched, as shown in Figure 25f,g.

4. Silicon layer is etched, as shown in Figure 25h.

5. Polyimide coat is deposited, to protect the top layer of the wafer during trench etching.

6. The bottom substrate Si and SiO_2 layers are etched, to release the MEMS.

7. Polyimide coat is removed, as shown in Figure 25i.
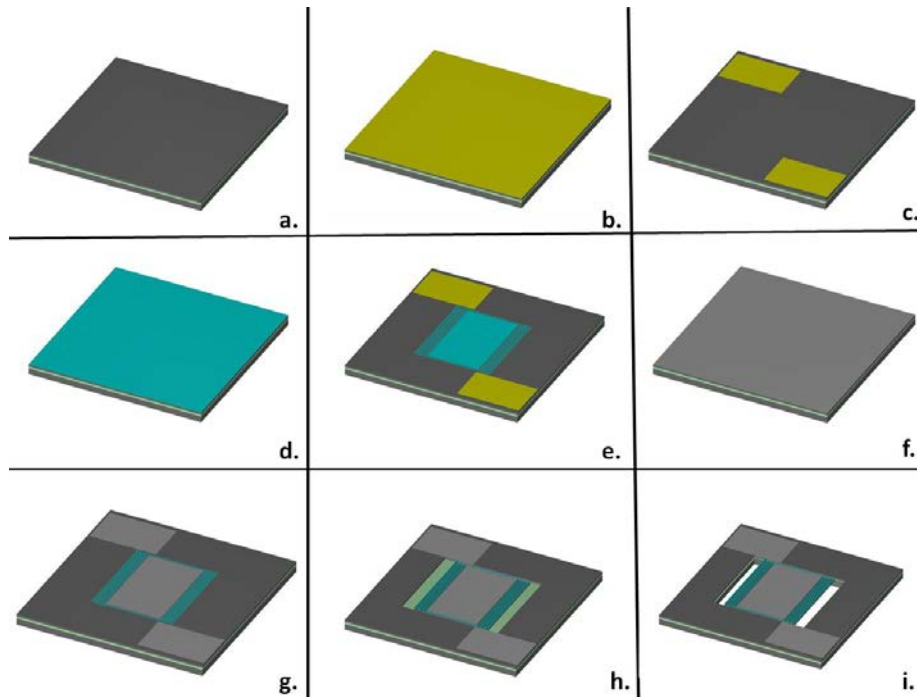
Figure 25.   The MEMSCAP PiezoMUMPS microfabrication. Silicon is shown in grey.
SiO$_2$ is shown in green. AlN is shown in blue.

VII. MEMS PROTOTYPE

While a proof of concept is ultimately the goal of successfully fabricating a piezoelectric energy harvesting MEMS, much effort has been taken to determine a successful and efficient means of MEMS fabrication. The piezoelectric effect is highly dependent on AlN directionality, as described in chapter III Section B. In section A of this chapter, three tests were performed to examine the crystal orientation of AlN layers for the NPS devices. Also, in Section A, data is collected to determine the conductivity of the AlN, which will affect how well a voltage is produced due to the flow of electrons in response to the piezoelectric effect. Finally, in Section B, the photolithography and AlN etching steps of the fabrication process are examined to ensure appropriate microfabrication.

A.   MATERIALS CHARACTERIZATION

Analysis in this section will include characterization of the material layers and device fabrication.

1.   AlN Characterization

Because crystal orientation is so significant for piezoelectric energy harvesting, determining the AlN orientation is necessary. In addition to AlN characterization, processing steps such as etching must be analyzed.

a.   *Etch Rate Analysis*

There is a relationship between etch rate and AlN crystal orientation. By recreating the etching conditions, we can compare the AlN etch rate of the energy harvester to the etch rates reported in reference [21]. This is achieved by timing the etching process and then measuring the AlN height via surface profilometry.   Figure 26 is an image of a surface profilometry measurement of AlN on Wafer 3 across a 6 legged spring structure. Table 3 summarizes the etch rate data for each wafer.
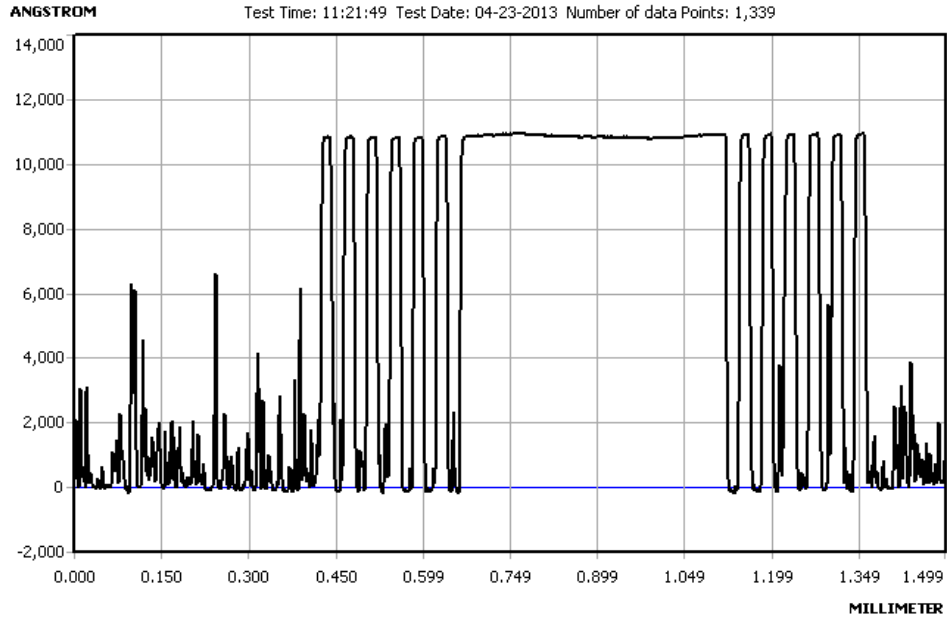
Figure 26.   Surface profilometry of AlN across a 6 legged spring structure.

Wafer	Etch Time [s]	AlN height [nm]	Etch Rate[nm/s]
3	64±1	1049.15	16.40
4	79±1	1075.02	13.61

Table 3.   A comparison of etch rate on Wafer 3 and Wafer 4. AlN height was obtained via surface profilometry.

Originally, an Arrhenius plot in reference [21] would be used to compare these etch rates to that of known crystal orientation. However, the experimental etch rates are beyond the scope of the data reported in [21].

b.   *Scanning Electron Microscopy*

Scanning Electron Microscopy, or SEM, can be used to verify and characterize the fabrication of the piezoelectric energy harvester. Also useful, the SEM can capture surface characteristics of the AlN layer [21]. AlN thin films with a high degree of c-axis orientation have a pebble type of topography. AlN thin films with (101)

orientation appear to have a more elliptic grain geometry [6]. SEM can be used to qualitatively characterize the AlN in the energy harvesting device.

Figure 27 is of the patterned AlN on SOI wafer, fabricated in the Naval Postgraduate School Clean Room. This image reveals an AlN topography consistent with the images associated with the c-axis, "pebble type," orientation.

Figure 28 shows a similar SEM image of AlN deposited under the same conditions on a single crystal Si wafer. In this figure are AlN grain size measurements that are also consistent with the reported 20–30nm grain size for c-axis AlN in resource [7].

| 4/16/2013 | HV | mag ☐ | WD | ⊢——— 500 nm ———⊣ |
| 9:39:30 AM | 5.00 kV | 205 000 x | 10.4 mm | Gregory structure 1 |
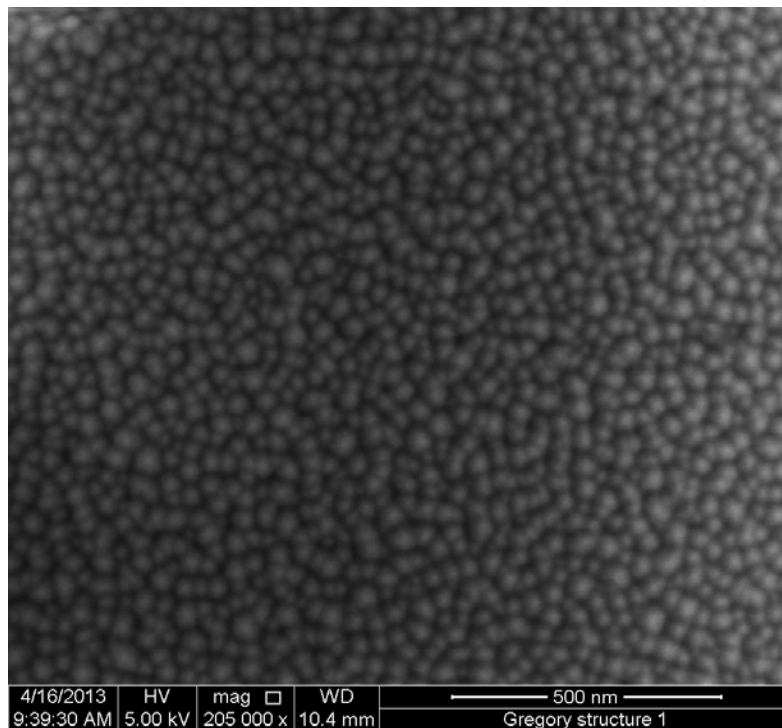
Figure 27.   SEM Micrograph of AlN used in NPS fabrication of energy harvesting MEMS.
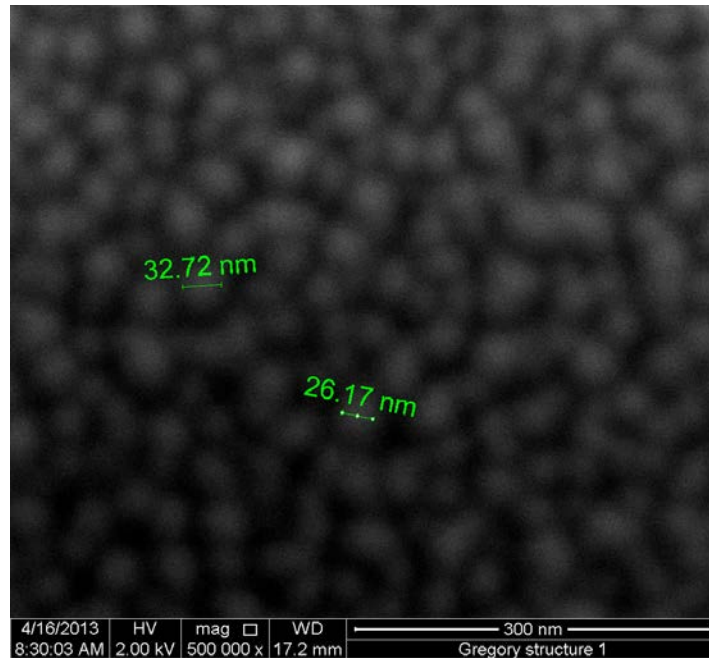
Figure 28.   SEM Micrograph at higher magnification of AlN used in NPS fabrication of energy harvesting MEMS.

c.   *X-ray Diffraction*

In past characterization of AlN thin films, X-ray Diffraction (XRD) has been a great tool for determining crystal orientation [6]. In reference [6], for AlN thin films with (002) orientation, an XRD revealed a 2θ measurement at 36 degrees. Figure 29 shows an XRD of the AlN on SOI used in this MEMS fabrication. The XRD patterns revealed in this chart indicate a high c-axis AlN orientation, which is optimal for use in piezoelectric devices.
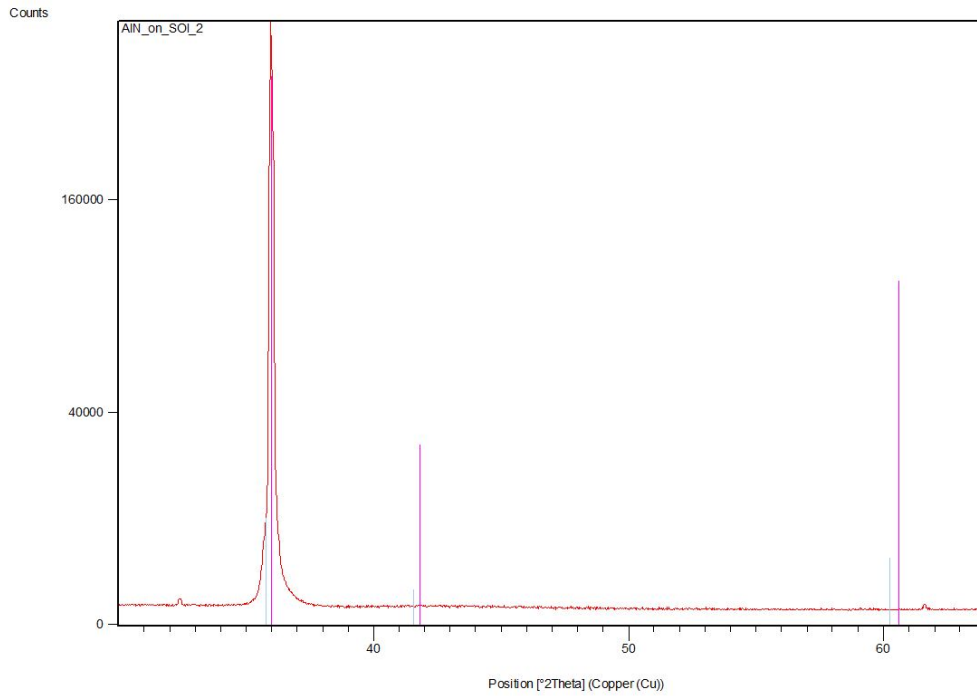
Figure 29.   XRD of AlN on SOI wafer. The red line indicates the XRD patterns, while the pink lines indicate predicted AlN peaks of various crystal orientations.

d.   AlN conductivity

The conductivity of a semiconductor is a measure of its ability to conduct electric current [8]. The conductance of an electric current is essential to the generation of electric power in this energy harvesting device, by means of an AC current from the piezoelectric effect of the vibrating MEMS. Table 4 shows the conductivity and resistivity of both Wafer 3 and Wafer 4.

	Resistivity (Ω cm)	Conductivity (S/m)
Wafer 3	80485.17	1.242×10^{-3}
Wafer 4	79440.44	1.259×10^{-3}

Table 4.   A summary of the AlN conductivity of SOI Wafer 3 and Wafer 4.

B.   FABRICATION ANALYSIS

The SPR 220-7, positive photoresist, was an effective mask for a device of this size, although some structural abnormalities arose when the SPR 220-7 was exposed to 400 or 500 Integra, which is a unit of UV power specific to the Canon PLA-501F contact aligner, used at NPS cleanroom to expose the photolithographic mask.   An effective etchant for AlN was 64 s to 79 s in 85% phosphoric acid (H_3PO_4) at 80°C. Figure 30 and Figure 31 provide an overview of the patterned AlN, the uppermost layer of the energy harvesting structures, on several wafers.   These pictures provide insight of the AlN etching process.
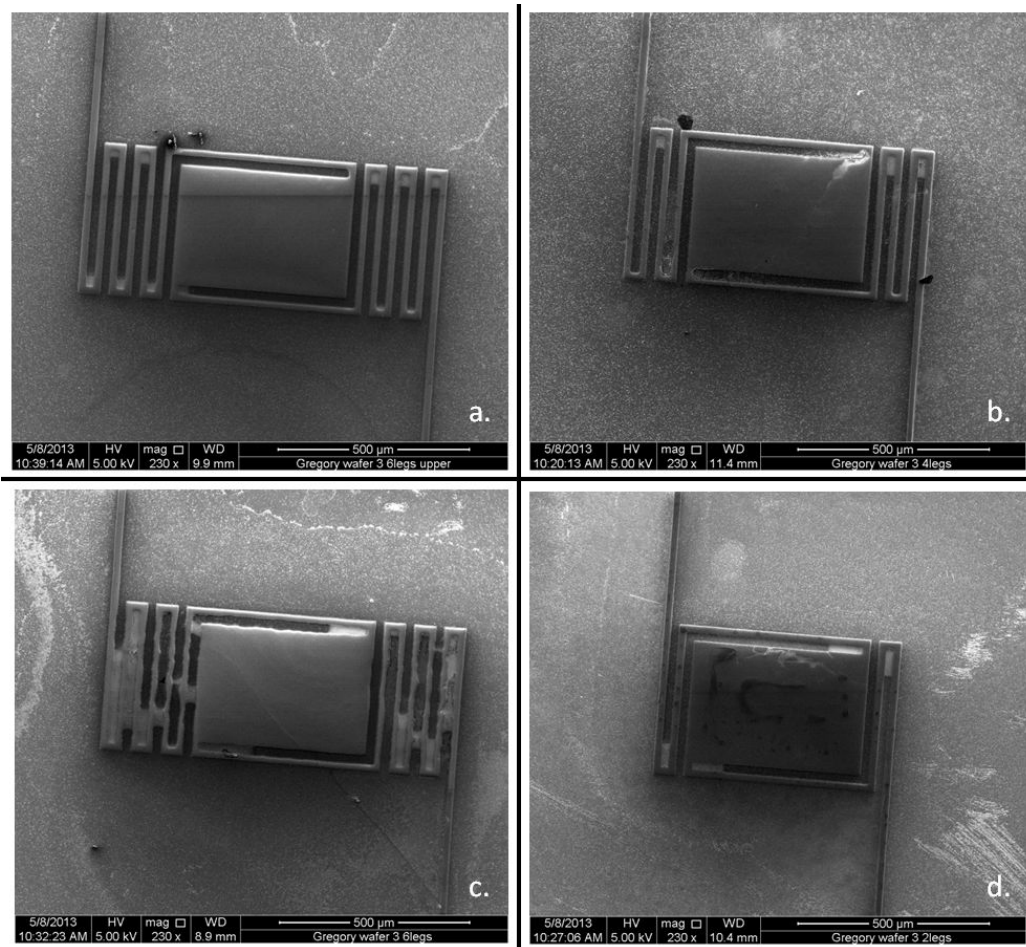
Figure 30.   SEM Images of NPS fabricated AlN structures on SOI wafer on Wafer 3. The Wafer 3 photoresist was exposed to 520 Integra. The AlN was etched in 85% H_3PO_4 at 80°C for 64 seconds.
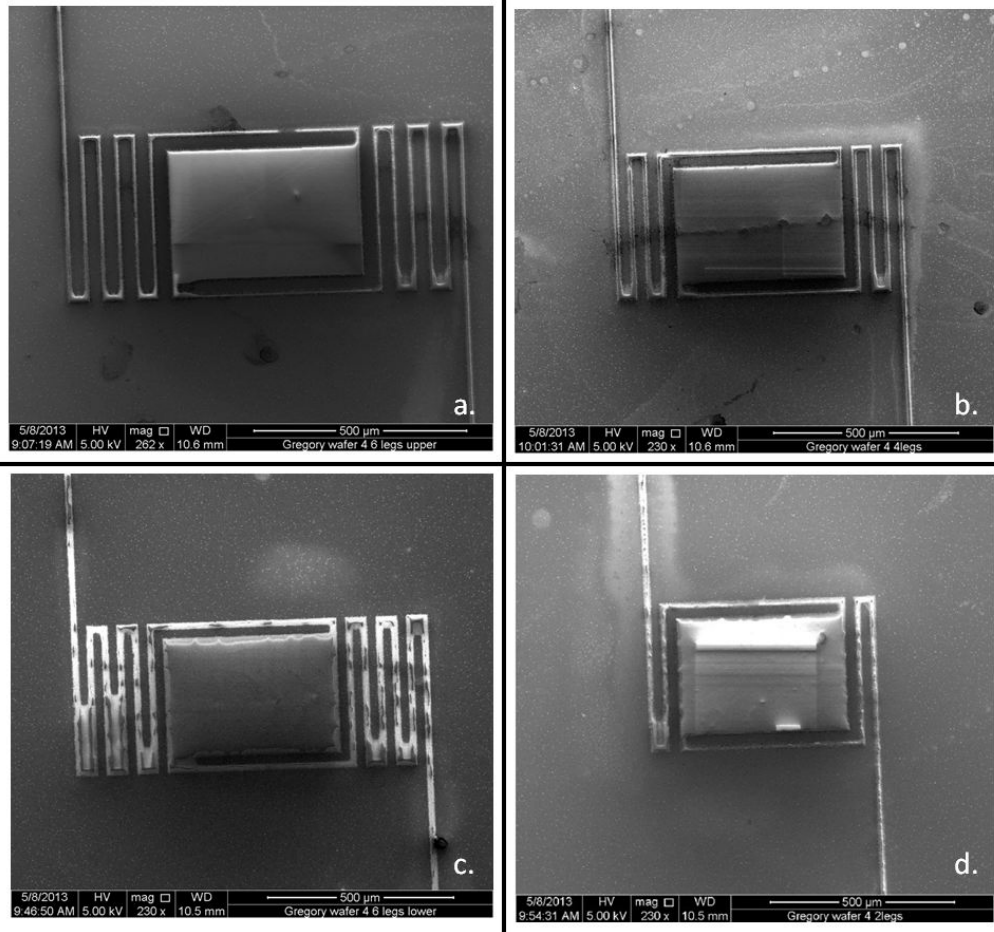
Figure 31.   SEM images of NPS fabricated AlN structures on SOI Wafer4. The Wafer 4 photoresist was exposed to 400 Integra. The AlN was etched in 85% H_3PO_4 at 80°C for 79 seconds.

The etching of the upper 6-legged structure, Figure 30a and Figure 31a, and the 4-legged structure, Figure 30b and Figure 31b, was successful in both fabrications. There are few abnormalities in these structures, when compared to the lower 6 legged structures, Figure 30c and Figure 31c, and the 2 legged structures, Figure 30d and Figure 31d. These structures have several places of uneven AlN, due to a poor exposure pattern. Figure 32 shows the lower 6 legged structure on Wafer 3 before the AlN etch, that provides insight to the poor results in etching this device.
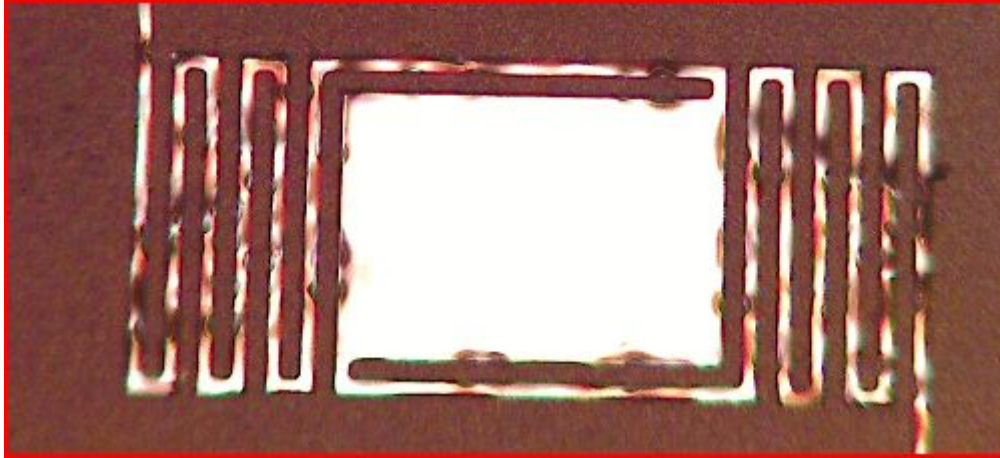
Figure 32.   Wafer 3 lower 6 legged structure. SPR 220-7 prior to H_3PO_4 etch. The uneven mask edges are due to overexposure of the photolithographic mask, which produced a "boiling" effect of the SPR 220-7.

This similar effect was found on the bottom two devices exposed at both 520 and 400 Integra. This is likely due to a nonuniform UV lamp in the contact aligner used for exposing the photoresist. The nonuniformity focused more power on the lower two devices during exposure, overexposing and essentially boiling the SPR 220-7. In a methodic analysis of the effect of the UV lamp on SPR 220-7, it was found that the ideal setting for exposure of SPR220-7 was 240-250 Integra. This setting is reflected in the unperformed fabrication steps listed in chapter VI section A of this thesis.

Because both wafers had the same abnormalities in the same areas of the wafers, the issue is most likely systemic in the photolithography, rather than in the etching of AlN. This indicates nonuniformities in the UV lamp. The poorly etched structures correlate to the same areas in the photoresist that developed abnormally, shown in Figure 32. These are expected to improve and expose uniformly patterned structures across the entire wafer once the problem with the lamp is addressed.

Even with a mask that avoided overexposure, there are still some etching anomalies that arose during the fabrication. In Figure 33, unetched AlN, seen as white spots between the structural legs, were seen in each of the spring structures on SOI Wafer 3. Compare this image to Figure 34, which is the same upper 6 legged structure as in

Figure 33, except that it is on SOI Wafer 4. In this image, the under etched AlN in the corners of the spring structure have been removed. However, there is significant thinning of the structural legs, due to over etching.
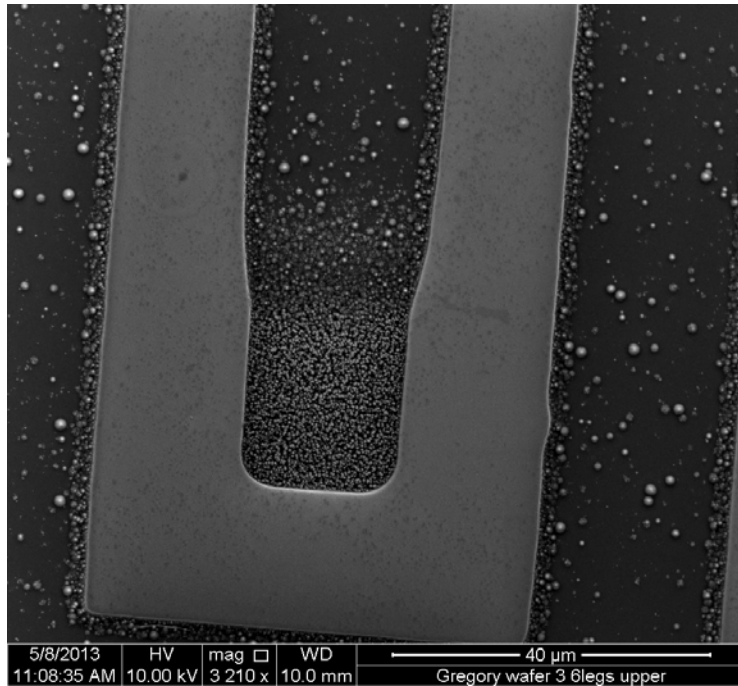
Figure 33.   Wafer 3 upper 6-legged structure. The "pebbly" by-product in the corner of the structure is unetched AlN.
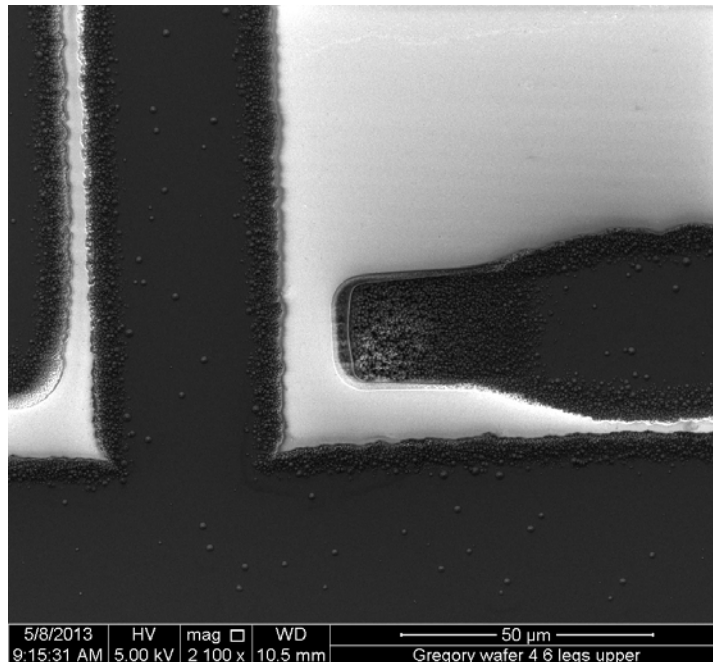
Figure 34.   Wafer 4 upper 6-legged structure. Note the significant thinning of the AlN leg off the main AlN pad due to a poor photolithographic mask, leading to over etching.

Table 5 displays the fabrication variables between Wafer 3 and Wafer 4. If one were to compare only the exposures of each wafer, it would be expected that Wafer 3 was over exposed and would result in over etched, or thin, structures. Conversely, Wafer 4 might be more underexposed, resulting in unetched AlN. However, it was Wafer 3 that retained unetched AlN, and Wafer 4 that was over etched. These results are likely due to the etch times. 64 seconds in the etchant was not quite enough to remove the AlN from the structure corners, whereas 79 seconds began to over etch the structural legs in Wafer 4.

Wafer	Etch Time [s]	Exposure [Integra]
3	64±1	520
4	79±1	400

Table 5.   A comparison of etch time and exposure for Wafer 3 and Wafer 4.

46

The most ideal structure was the upper 6 legged energy harvester on Wafer 3, show in Figure 35. While there remains some unetched AlN in the corner of each structural leg, the legs themselves were not over etched, as shown in the same structure on Wafer 4. The unetched corners on Wafer 3 are likely an effect of the over developed photoresist, while the over etched legs on Wafer 4 are most likely due to the extra 15 seconds in the H_3PO_4 etchant.

| 5/8/2013 | HV | mag □ | WD | —————— 500 μm —————— |
| 10:39:14 AM | 5.00 kV | 230 x | 9.9 mm | Gregory wafer 3 6legs upper |

Figure 35.   Wafer 3 upper 6-legged structure.

At the completion of this thesis, the MEMSCAP devices have been fabricated and are being prepared for shipment to NPS. Analysis of these piezoelectric energy harvesters will be addressed in Chapter IX, Future Work.

THIS PAGE INTENTIONALLY LEFT BLANK

VIII. SUMMARY SECTION

The work in this thesis concluded with the successful design and fabrication of a piezoelectric energy harvesting MEMS through the effective etching of AlN. This work included extensive design optimization through COMSOL modeling, designed a MEMS model, close to 60 Hz resonant frequency for fabrication through the PiezoMUMPS program and conforming to the PiezoMUMPS design rules, char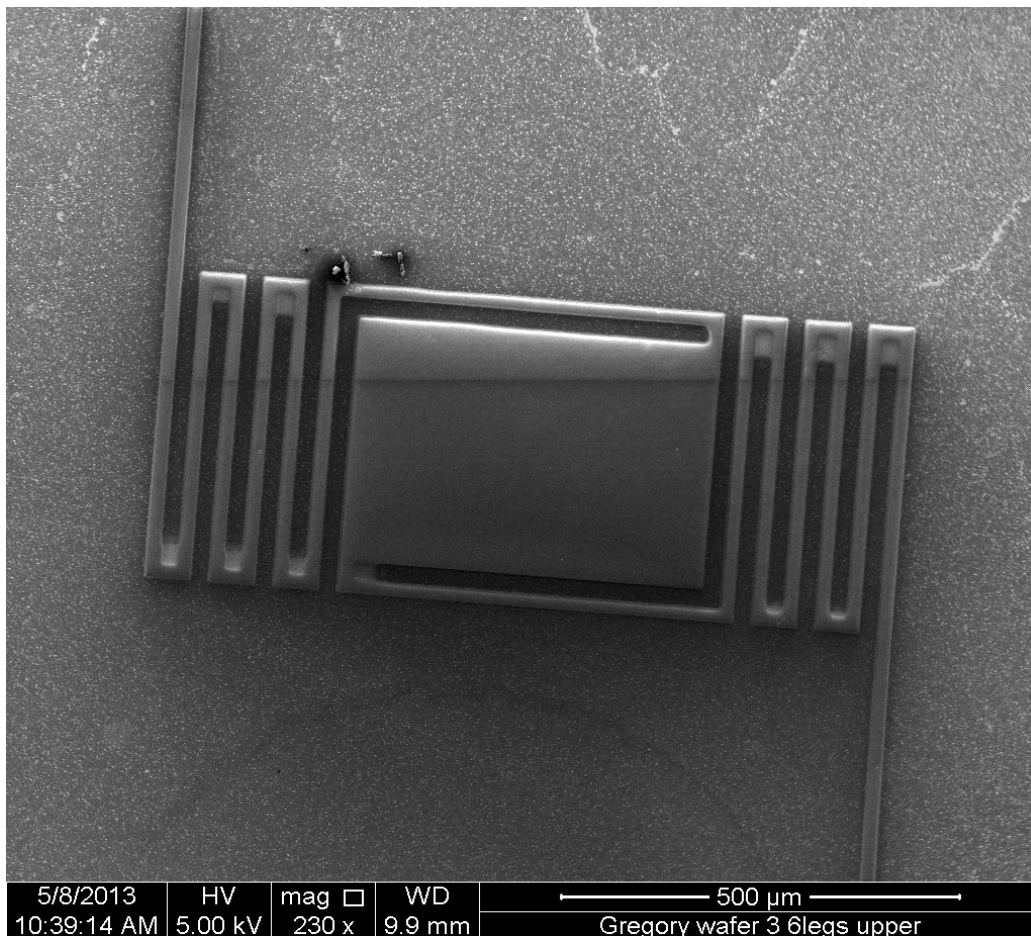acterized the device materials, developed a fabrication procedure for use in the NPS Clean Room, and began the implementation of that fabrication procedure.

This thesis has produced reproducible COMSOL models for the physical testing of the piezoelectric energy harvesting devices mentioned throughout the work. The COMSOL models specifically demonstrate the ability to quickly analyze a MEMS device without requiring the long lead-time of fabricating the device before testing. The modeling in this thesis has laid the groundwork for future work in this area of electrical energy production by means of MEMS devices. The models produced will serve as the basis for future generations of devices, as well as the testing of other MEMS devices designed at NPS.

At the conclusion of this thesis research, both the high frequency and the low frequency models submitted to MEMSCAP for the PiezoMUMPS program have been fabricated and are being prepared for shipment. In coming months, the energy harvesting concept will be demonstrated with these models via the vibrational testing procedure described in Chapter IX.

Much of the data collected for the characterization of the NPS device materials, Chapter VII Section A, was intended to determine the crystal orientation of the AlN. A single crystal with principal axis (002) orientation is ideal for this MEMS design. The SEM images of the AlN grains indicate a principal axis orientation. Also, the XRD pattern shows a single peak at 36 degrees, suggesting that the AlN has a high principal axis orientation.

The NPS fabrication procedure, described in Chapter VI section A, was completed through step 7. The procedure allowed for a successful application of the SPR 220-7 photolithographic mask. The mask was sufficiently exposed, allowing for a useful mask in etching the AlN. An effective etchant for AlN was 85% H_3PO_4 at 85°C. From the fabrication analysis in Chapter VII, it has been demonstrated that parts of the fabrication process need to be honed to a more specific procedure for optimal results. Specifically, the photolithographic mask must be exposed at a lower Integra setting to prevent SPR 220-7 overexposure and boiling. Also, the time the wafer is immersed in the AlN etchant needs to be further evaluated, as 64 seconds under etched the spring structure which may alter the resonant frequency and the devices spring constant, and 79 seconds over etched the AlN, sacrificing the integrity of the structural legs.

While not all of the microfabrication steps have been completed, the most critical fabrication aspect, AlN etching has been significantly defined. The other steps prescribed in Chapter IV are well-known, standardized processes.

IX. FUTURE WORK

Further work on piezoelectric energy harvesting MEMS is necessary, not only to complete the MEMS fabrication and test the model, but also to optimize the MEMS design and hone the fabrication process for favorable results.

A. MODELING

COMOSOL modeling has yielded theoretical values for the MEMS devices fabricated at NPS and PiezoMUMPS, such as eigenfrequency, open-ended voltage, device displacement, and electrical power production. Successful modeling has brought forth optimized device dimensions in order for the MEMS to resonate at 60 Hz, operating frequency of the LM2500 Gas Turbine Engine [5]. Once a piezoelectric energy harvesting device is fabricated, experimental testing can verify the results of the COMSOL modeling, allowing for adjustments of piezoelectric properties and realistic mechanical parameters that were not easily available, such as the Rayleigh damping coefficients. For future designs, COMSOL modeling should be used to further optimize the dimensions of the MEMS in order to increase electrical power output while simultaneously lowering the overall footprint of the device. In order for this technology to make a larger impact for the Department of the Navy, further modeling is needed to design a MEMS that is tunable to many frequencies. Further modeling is also needed in order to determine the lifecycle of the devices, in terms of the stress experienced at the joints of the MEMS devices. By verifying the modeling results with experimental testing, the efficiency of the mechanical to electrical energy conversion occurring in the MEMS devices can be obtained.

B. FABRICATION

The PiezoMUMPS models have been fabricated. After a successful shipment from MEMSCAP to the Naval Postgraduate School, the output of those devices can be tested.

The NPS Fabrication Process needs to continue with Wafer 3 and Wafer 4, picking up at step 8, reactive ion etching of the top layer of silicon around the AlN structures and subsequent trench etching to release the structure.

For the next generation of energy harvesting MEMS, the following recommendations should be implemented to improve the device fabrication:

- In exposing the SPR 220-7 photolithographic mask, 400-500 Integra will over expose the mask and compromise some of the structures. From a series of trial runs of SPR 220-7 on dummy wafers, the ideal exposure setting is 240 Integra.

- CD-26, the photolithographic mask developer, etches AlN. Though it is an anisotropic etchant [22], in a previous fabrication the CD-26 etched away the AlN leg structures, leaving only isolated AlN pads. Wafers 3 and 4 were developed for 4 to 7 minutes in the CD-26 with minimal AlN etching.

- SPR 220-7 tends to swell with environmental moisture after it has been applied, exposed, and developed. Though 7 to 8 microns of the mask was applied, after a few days on a wafer, surface profilometry measured 10 to 11 microns difference between the AlN and the top of the mask. This mask swelling may mar the more fine details of the MEMS design. As such, it is recommended to minimize the wait time between developing the mask and etching the AlN.

- As discussed in Chapter VII, 85% H_3PO_4 at 80°C was an effective AlN etchant. As seen in the SEM images of both wafers, Wafer 3 was under etched at 64 seconds in H_3PO_4, and Wafer 4 was over etched at 79 seconds in H_3PO_4. More testing needs to be done to narrow the etching time down to a range of one or two seconds, for optimized fabrication.

C. TESTING

Once a piezoelectric energy harvesting MEMS is successfully fabricated, either through the PiezoMUMPS program or in the NPS Clean Room, the output voltage can be measured. By connecting a frequency generator to a mechanical shaker, it can be made to vibrate at the MEMS device's resonant frequency, 60 Hz. The voltage difference can be measured across the device by soldering a wire to the metal pads on either end of the energy harvester, and connecting the wires to a voltmeter while the device is vibrated at 60 Hz.

LIST OF REFERENCES

[1]   U. S. Government, Office of the Press Secretary, "Executive order 13514: Federal leadership in environmental and economic performance," BiblioGov, Washington D.C., 2009.

[2]   United States Marine Corps, "United States Marine Corps expeditionary energy strategy and implementation plan," Marine Corps Expeditionary Office, Washington D.C., 2011.

[3]   U. S. Government, Federal Register, "Executive order 13423 of January 24, 2007: Strengthening federal environmental, energy, and transportation management," 2007.

[4]   C. Richards and M. Anderson, "Efficiency of energy conversion for devices containing a piezoelectric component," *Journal of Micromechanics and Microengineering*, vol. 14, p. 717, 2004.

[5]   "Gas turbine systems technician (electrical) 3/ gas turbine systems technician (mechanical) 3," NAVEDTRA 14114, vol. 2, p. 2-1, 1991.

[6]   A. Ababneh and G. Marchand, "Comparison between AlN thin films with different crystal orientation for MEMS applications," *Smart Sensors, Actuators, and MEMS IV*, SPIE, vol. 7362, pp. 1–7, 2009.

[7]   "SOIMUMPS," MEMSCAP, [Online]. Available: http://www.memscap.com/products/mumps/soimumps. [Accessed 24 April 2013]

[8]   C. Liu, *Foundations of MEMS*, Upper Saddle River, NJ: Pearson Education, Inc., 2006.

[9]   D. Baughman, "Creation and optimization of novel solar cell power via bimaterial piezoelectric MEMS device," Monterey, CA: Naval Postgraduate School, 2011.

[10]   S. Roundy, P. K. Wright and J. Rabaey, "A study of low level vibrations as a power source for wireless sensor nodes," Berkeley, CA: University of California, Berkeley, 2002.

[11]   A. Kasyap, "Development of MEMS-based piezoelectric cantilever arrays for vibrational energy harvesting," Gainesville, FL: University of Florida, 2007.

[12]   S. O. Kasap, *Electronic materials and devices*, New York: McGraw-Hill, 2006.

[13]   A. Townley, "Vibrational energy harvesting using MEMS piezoelectric generators," University of Pennsylvania.

[14]   Piezo Systems, Inc., "Introduction to piezoelectricity," Woburn, MA: Piezo Systems, 2011.

[15]   "OEM Group," OEM Group, Inc., 2011. [Online]. Available: www.oemgroupinc.com. [Accessed 24 April 2013].

[16]   A. Cowen, G. Hames, K. Glukh and B. Hardy, *PiezoMUMPs Design Handbook Revision 1.0*, MEMSCAP Inc., 2012.

[17]   Y. Shu and I. Lien, "Efficiency of energy conversion for a piezoelectric power harvesting system," National Taiwan University, Taipei: Institute of Applied Mechanics, 2006.

[18]   V. V. Felmetsger and P. N. Laptev, "New generation of S-gun magnetron for AlN reactive sputtering," Petaluma, CA: Tegal Corporation, 2010.

[19]   MicroChem Corporation, Material Safety Data Sheet for MCC Primer 80/20, Newton, MA: MicroChem Corporation, 2005.

[20]   D. Grbovic, N. V. Lavrik, S. Rajic and P. G. Datskos, "Arrays of SiO2 substrate-free micromechanical uncooled infrared and teraherts detectors," *Journal of Applied Physics*, vol. 104, pp. 054508-1-054508-7, 2008.

[21]   A. Ababneh, H. Kreher and U. Schmid, "Etching behaviour of sputter-deposited aluminium nitried thin films in H3PO4 and KOH solutions," Microsyst Technol, vol. 14, pp. 567-573, 2008.

[22]   S. Saravanan, E. Berenschot, G. Krijen and M. Elwenspoek, "A novel surface micromachining process to fabricate AlN unimorph suspensions and its application for RF resonators," *Sensors and Actuators*, pp. 340–345, 2006.

[23]   A. Phipps and D. Phung, "Development of kinetic energy harvesting systems for vehicle applications," SPAWAR Systems Pacific.

[24]   R. Elfrink and M. Renaud, "Vacuum-packaged piezoelectric vibration energy harvesters; damping contributions and autonomy for a wireless sensor system," IMEC/ Holst Centre, stacks.iop.org/JMM/20/104001, 2010.

[25]   Oak Ridge National Laboratory, [Online]. Available: http://www.ornl.gov/sci/nstl/index.htm. [Accessed 24 April 2013]

[26]   "Energy independence and security act of 2007," United States Senate and House of Representatives, 2007. [Online] Available: http://www1.eere.energy.gov/femp/regulations/eisa.html. [Accessed March 1, 2013].

[27] V. V. Felmetsger, P. N. Laptev and S. M. Tanner, "Crystal orientation and Stress in AC reactively sputtered AlN films on mo electrodes for electro-acoustic devices," in IEEE International Ultrasonics Symposium, 2008.

[28] S. M. Forester, "Energy harvesting for self-powered, ultra-low power microsystems with a focus on vibration-based electromechanical conversion," Monterey, CA: Naval Postgraduate School, 2009.

[29] S. P. Beepy, M. J. Tudor and N. M. White, "Energy harvesting vibration sources for microsystems applications," Southhampton SO17 IBJ, United Kingdom: University of Southhampton, 2006.

[30] S. Prasanna and S. M. Spearing, "Materials selection and design of bimaterial actuators," *Journal of Microelectromechanical Systems*, vol. 16, no. 2, 2007.

[31] E. Iborra, J. Olivares, M. Clement and L. Vergara, "Piezoelectric properties and residual stress of sputtered AlN thin films for MEMS applications," *Sensors and Actuators*, pp. 501–507, 2004.

[32] S. Afrang and G. Rezazadeh, "Design and simulation of simple and varying section cantilever and fixed-fixed end types MEMS switches," in ICSE 2004 Proceedings, Kuala Lumpur, Malaysia, 2004.

[33] V. V. Felmetsger, P. N. Laptev and R. J. Graham, "Deposition of ultrathin AlN films for high frequency electroacoustic devices," JVSTA, pp. 021012-1-7, Mar/Apr 2011.

[34] S. D. Jian Zhou, H. Jin, B. Feng and D. Wang, "Flexible surface acoustic wave device with AlN film on polymer substrate," *Journal of Control Science and Engineering*, vol. 2012, p. 5, 2012.

THIS PAGE INTENTIONALLY LEFT BLANK

INITIAL DISTRIBUTION LIST

1.   Defense Technical Information Center
        Ft. Belvoir, Virginia

2.   Dudley Knox Library
        Naval Postgraduate School
        Monterey, California